sustainability

MDPI

Review

A Review of Modeling Rotating Packed Beds and Improving Their Parameters: Gas–Liquid Contact

Farhad Ghadyanlou [1], Ahmad Azari [1,*] and Ali Vatani [2]

[1] Faculty of Petroleum, Gas and Petrochemical Engineering, Persian Gulf University, Bushehr P.O. Box 75169-13817, Iran; ghadyanlou@gmail.com
[2] School of Chemical Engineering and Institute of LNG, College of Engineering, University of Tehran, Tehran P.O. Box 14779-56315, Iran; avatani@ut.ac.ir
* Correspondence: azari.ahmad@gmail.com or azari.ahmad@pgu.ac.ir; Tel.: +98-917-323-8639; Fax: +98-773-344-5182

Abstract: The aim of this review is to investigate a kind of process intensification equipment called a rotating packed bed (RPB), which improves transport via centrifugal force in the gas–liquid field, especially by absorption. Different types of RPB, and their advantages and effects on hydrodynamics, mass transfer, and power consumption under available models, are analyzed. Moreover, different approaches to the modeling of RPB are discussed, their mass transfer characteristics and hydrodynamic features are compared, and all models are reviewed. A dimensional analysis showed that suitable dimensionless numbers could make for a more realistic definition of the system, and could be used for prototype scale-up and benchmarking purposes. Additionally, comparisons of the results demonstrated that *Re*, *Gr*, *Sc*, *Fr*, *We*, and shape factors are effective. In addition, a study of mass transfer models revealed that the contact zone was the main area of interest in previous studies, and this zone was not evaluated in the same way as packed beds. Moreover, CFD studies revealed that the realizable k-ε turbulence model and the *VOF* two-phase model, combined with experimental reaction or mass transfer equations for analyzing hydrodynamic and mass transfer coefficients, could help define an RPB system in a more realistic way.

Keywords: absorption; HiGee; CFD; intensification; hydrodynamics

Citation: Ghadyanlou, F.; Azari, A.; Vatani, A. A Review of Modeling Rotating Packed Beds and Improving Their Parameters: Gas–Liquid Contact. *Sustainability* **2021**, *13*, 8046. https://doi.org/10.3390/su13148046

Academic Editors: Ahmed Elreedy and Mohamed Elsamadony

Received: 28 May 2021
Accepted: 13 July 2021
Published: 19 July 2021

1. Introduction

Process intensification (PI) is defined as an engineering application utilized to improve sustainability, cleaning, safety and energy efficiency. PI in mass transfer (MT) involves three main methods: rotating, mixing, and vibrating [1]. There are good reviews available on PI that provide more details on this topic [2,3]. Researchers have been using the advantages of centrifugal fields for more than 65 years [4]. A rotating packed bed (RPB) contactor is a piece of PI equipment, also called a "HiGee" (high g) because of the high gravity applied in this contactor by the centrifugal force used for increasing the contact of phases [5]. This device was first patented in 1963, and includes concentric rings for packing purposes [6]. Industrial applications of this equipment started in the 1970s when Imperial Chemical Industries worked on technology derived from NASA research projects [7]. Almost a decade later, Ramshaw and Mallinson presented a report on NH_3 absorption and MT coefficient intensification using an RPB for the first time [8]; later, this technology was licensed by Glitsch in the USA [9]. Investigations into and the development of RPBs were have been out by numerous researchers in many MT and reaction fields, such as distillation. Several kinds of RPB have been reviewed and their advantages discussed in [10], while the results and some of their industrial applications are presented in [11].

As CO_2 emissions are now a global concern, investigations in this field employ three main approaches: post-combustion, oxy-fuel combustion, and pre-combustion for CO_2 capture [12,13]. Chemical absorption has been applied and developed more extensively in

post-combustion than in other industrial processes [14]. Therefore, a large amount of waste is produced by the use of certain conventional gas treatment packed bed columns (PBCs), and this approach requires high quantities of absorbent solvents in order to prevent hydrate formation with the small quantities of other components, such as CO_2 and H_2S. The most common acidic gas removal problems include absorption heat, high energy consumption for regeneration, and amine solutions' corrosive nature and temporal degradation [15,16]. The previous field studies on chemical absorption will be explained, along with some brief examples, below.

1. Absorbent formulation, in which a highly soluble, reactive, absorbent, and aqueous solution of alkanolamines is made and blended by adding activators or promoters, such as sterically hindered amine *AMP*, and effective promoters, such as *PZ*.
2. Process intensification involves the application of PI techniques or devices and optimization parameters. This category contains many techniques that can be considered to enhance transport in numerous processes, such as bioremediation [17], water deaeration [18], and absorption. As regards devices, many popular contactors are available, such as rotating discs, membranes, and RPBs.

For instance, Hosseinzadeh et al. [19] examined CO_2 capture with a hallow fiber membrane contactor (HFMC), using *MEA* to increase the chemical reaction rate and the contact of phases. M. Theils et al. [20] performed a comparison between several arrangements of PBs and RPBs, and demonstrated that reducing the packing volume in the RPBs resulted in equal removal efficiencies. Additionally, this kind of method is applied in many fields, and the simultaneous application of the above two intensifying absorption methods (a and b) can offer advantages such as energy reduction in thermal regeneration using an RPB on *MEA*–CO_2 system, as reported by Cheng et al. [21]. Their results show that the same regeneration efficiency in PBCs could be achieved with RPBs that were at least 10 times smaller than the PBCs, and they demonstrated that RPBs had higher MT and heat transfer coefficients and involved less *HTU* and regeneration energy consumption. Other benefits of this approach have also been reported. An investigation into CO_2 capture with water-based NFs (absorbing solutions) in HFMC revealed possible enhancements to MT and removal efficiency [22]. In addition, Luo et al. [23] reported that the relative effective gas–liquid interfacial surface area and volumetric liquid-side MT coefficient were both increased when using ultrasonic induction, in comparison with an RPB without ultrasonic induction under the same conditions. These approaches, referred to as hybrid processes, have been further discussed in [24].

RPB is a piece of equipment that operates via centrifugal acceleration, which affects the hydrodynamics to induce PI. Therefore, improving an RPB's characteristics via hydrodynamic analysis is the main goal of this investigation. In this paper, the status of the gas–liquid contact in the RPB, and especially the absorption processes taking place in various models and methods, have been evaluated and reviewed. The comparison of publications shows that various configurations of RPBs have been developed to expand contact zones and effective surface areas, and to achieve a higher MT and capacity, as well as a reduced pressure drop.

In the first section, the main concepts, such as the advantages of centrifugal gravity, the geometry and classification of RPB, the directions of investigations (i.e., hydrodynamic and mass transfer enhancement) and modeling outlooks, are described. In the second section, the modeling of hydrodynamic parameters and their development to attain accurate systems are analyzed. In the third section, the developments in the modeling of MT's parameters as regards its rate are studied. Finally, in the last sections, two powerful methods suitable for hydrodynamic analysis and scaling-up, as well as the effects of centrifugal gravity on the dimensionless numbers that form the main focus of this analysis, are reviewed and evaluated. Here, all the above-mentioned items are reviewed simultaneously, because no previous review has evaluated all the parameters that together characterize the RPB.

2. RPB Advantages and Configurations

An RPB contactor consists of packing mounted on a horizontal/vertical shaft (rotor), casing, and a liquid distributor. A simple conventional RPB is made up of a rotor enclosed in casing, with a liquid distributor that injects liquid into the packing center. The packing is divided into three zones: the bulk packing, the end-effect (the part near the inner edge of the rotor), and cavity zones, which are between the outer edge of the packing and the inner edge of the casing [25]. The acceleration in RPBs (typically 1000 g) is greater than that in PBCs, which allows for improved micro-mixing, as demonstrated, for instance, by the experimental results of Yue's investigation of an RPB [26]. The high gravity leads to higher gas–liquid interfacial surface area accessibility in RPBs, compared with conventional PBCs.

Ramashaw and Mallinson applied average centrifugal accelerations of up to $1000\times g$, and showed that the MT coefficient would increase by ω, with a power of 0.28–1.08 [8]. This was confirmed in other studies, such as those by Guo et al. [27] and Liu et al. [28], and in reports on MT coefficients, which examined parameters of 1500 rpm and higher. Tsai et al. conducted a similar experiment and added 38% to the MT coefficient's value, with an annular speed increase from 600 to 1800. They reported that this was due to the boundary layer thickness reduction [29]. On the other hand, the liquid film becomes thinner with higher annular speeds and greater radii from the axis, due to the lower difference between the phase interface and average bulk concentrations [30]. Additionally, the effective surface has been shown to increase with an increase in the ω [31]. Lin et al. examined the effective surface area, which they increased from 5.9 to 31.7 m^2/m^3 by increasing the rotational speed from 600 to 1800 rpm [32].

Chen et al. examined the liquid hold-up in two RPBs with different sizes of packing and with rotations of 300–1500 rpm (providing 4–152 g), and showed that the liquid hold-up was reduced with an increase in ω [33]. The MT rate directly depends on hold-up, which is a function of the rotational speed, and ω directly depends on the radius of the packing [34]. Furthermore, the rate of pressure drop within the RPB increases with an increased rpm, as illustrated by the results of Zheng et al. and Sandalia et al. [35,36]. Additionally, as examined and discussed in [37,38], the height of transfer unit (*HTU*) achieved in an RPB is lower than that in a PBC under the same conditions.

Some researchers focused on acidic gas removal efficiency, showing that it increased with an increase in the rpm [39,40]. Moreover, Thiels et al. [20] demonstrated that a lower packing volume was required at higher rpms than at lower ones to achieve the same value of removal efficiency.

Based on the above information and in order to optimize the RPBs, many researchers have refined the operation parameters of RPB contactors by focusing on increasing the contact between the phases and staging, which allows better feed injection between the stages and increases the capacity of the contactor. A summary of US patents registered in 1935–2018 is given in Table 1, which shows that US patent development has been focusing on modifying RPBs to increase their contact zone. More detailed information about several patents can be found in [6].

Table 1. US RPB patents published in 1939–2018.

Type of Rotor	CCF	Improvements	Patent No.	Inventor(s)	Published Year
Single	CC	Contact zone and seals	US 2,172,222	W. J. Podbielniak [41]	1939
		Contact zone	US 2,281,796	W. J. Podbielniak [42]	1935
			US 2,758,783	W. J. Podbielniak [43]	1951
			US 2,878,993	W. J. Podbielniak [44]	1959
			US 2,941,872	C. W. Pilo et al. [45]	1960
			US 3,034,730	C. W. Pilo et al. [46]	1962
		Contact zone, reduced entrainment	US 3,233,880	W. J. Podbielniak [47]	1962
Multi-rotor		Contact zone, increased capacity	US 3,344,981	W. J. Podbielniak [48]	1965
Single		Contact zone	US 3,415,501	C. W. Pilo et al. [49]	1965
Multi-rotor		Contact zone, increased capacity	US 3,486,743	D. B. Todd [50]	1967
Single	CC & COC	Contact zone	US 4,283,255	C. Ramshaw and R. H. Mallinson [8]	1981
Single	CC		US 4,397,794	C. W. Pilo [51]	1981
Single		Liquid distribution and contact zone	US 6,884,401 B2	S. Yang et al. [52]	2002
Multi-rotor		Contact zone	US 7,344,126 B2	J Ji et al. [53]	2004
Single	CC & COC		US 8,448,926 B2	M. D. Mello et al. [54]	2011
Multi-rotor			US 20130319235A1	H. Wolf et al. [55]	2012
Single	CC		US 20160317967 A1	M. Kotagiri et al. [56]	2016
Single			US 20170028311A1	B. K. Namdeo et al. [57]	2017
Two stages			US 20170157554A1	C. H. Yu and C. S Tan [58]	2017
Multi-rotor	CC & COC		US20180016159A1	M. V. D. e Mello et al. [59]	2018

CCF: contacting conditions of fluids; CC: counter-current; COC: co-current; MTP: mass transfer process.

The different RPB names depend on the structure of the rotor, e.g., baffle [29] and blade [60], the bulk zones of which consist of baffles or blades, respectively; split (*RSB*) [61], the rotor of which includes dual packings rotating in the same or opposite directions; zigzag (*RZB*), which comprises a special rotor with a zigzag flow direction [62].

Generally, RPBs can be classified according to six criteria, as shown in Figure 1.

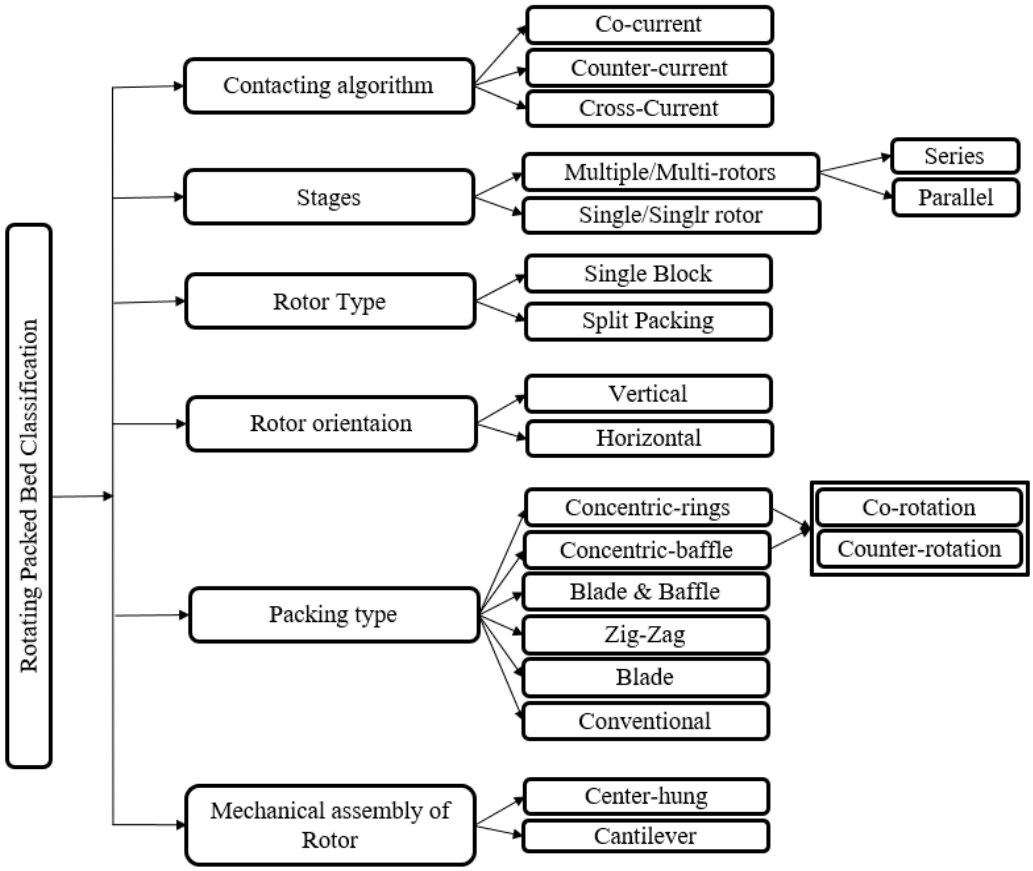

Figure 1. RPB categories.

Comparing the cross-current and countercurrent flows of simple RPBs, Chia-Chang Lin et al. investigated CO_2 removal using caustic solution, and reported that the K_Ga values of the cross-current flows were higher than those of the countercurrent flows [63]. In the same year, G. Q. Wang et al. [62] developed *RZB*s with similar MT efficiency and better operability and turn-down ratios. This contactor was first patented in 1952 by Kapitza [64]. After consulting the review papers of Visscher et al. [65] and Wang et al. [66], which were published in 2013 and 2019, respectively, the advantages of *RZB*s over simple RPBs may be listed as follows:

1. less maintenance due to their static seal;
2. possibility of multiple feeds and more flexibility;
3. no need for liquid distributers;
4. more liquid hold-up and residence time;
5. multi-rotor operability on one shaft.

Additionally, Wang et al. [67] contributed to *RZB* optimization by making modifications to its structure.

The disadvantages of this kind of RPB in comparison with simple RPBs include a lower MT rate, which is attributed to the replacement of packings with baffles and rings, and higher power consumption.

RPBs equipped with blades and RPBs with a number of liquid inlets have greater MT efficiency than simple RPBs due to the intensified MT rate in their end-effect zone, as Guang-Wen Chu et al. reported [68].

Moreover, counter-rotation *RSB*s achieve greater MT efficiency than the co-rotation type [69]. Furthermore, the benefits of an *RZB* over an RPB include the possibility of additional feed streams, the replacement of a dynamic seal with a static one, the need for fewer liquid streams for distributers, greater liquid hold-up, and the operability of stages by one rotor [65].

Different layouts with RPBs or PBCs in series or in parallel may help to achieve specific process parameters [70]. For instance, C. H. Yu et al. [71] studied the effect and removal efficiency of these configurations by examining eight single-, parallel- and series-mode configurations of RPBs and PBCs with *MEA*, and showed that the greatest level of gas treatment was achieved with two RPBs in a parallel mode, the regeneration energy consumption of which was approximately equal to that of a PB.

3. Modeling Rotating Packed Beds

RPB contactors can be modeled via various approaches based on the MT's characteristics and hydrodynamic analysis, as shown in Figure 2. Theoretical and mechanical models help us to comprehend the nature of gas–liquid flows and reactions. These methods result in significant discrepancies with experimental data due to the simplification of assumptions. Statistical and empirical methods developed to increase accuracy rely on semi-empirical and statistical regressions. Generally, these models give acceptable results, but due to their dependency on experimental data, it is not possible to infer general correlations from these models. Numerical simulation is another useful approach, and it is categorized into chemical-based and computational fluid dynamics-based (CFD) types, which are more detailed and accurate in comparison with previous methods [72]. Additionally, in the context of CFD complexity and the numbers of empirical model errors, machine learning, or artificial intelligence, is another method that has been developed by researchers such as Saha, who used artificial neural networks (ANN) to estimate the overall gaseous MT coefficient by applying the radial basis transfer function [73]. Lashkarbolooki et al. [74] employed ANN for pressure drop modeling and estimation in RPBs under various operations. Zhao et al. [75] proposed an intelligent approach to MT coefficient estimation in CO_2–NaOH systems by employing the radial basis transfer function. Saha reported that the developed model was more accurate than multiple nonlinear regression and ANN. Li et al. [76] applied three ANN models to simulate adsorption in RPBs. Liu et al. [77] developed an ANN-based approach for biosorption modeling, which was used the Re_L, λ, maximum contact time, ratio of particle diameter to bed height ($D_{particle}/Z$), and ratio of initial concentration to packing density, as input variables. Recently, Liu et al. employed ANN to a model and estimated the overall MT coefficient (K_La) in the ozone absorption process in RPBs, using input variables such as Re_G, Re_L, Fr_L, and We_L. [78].

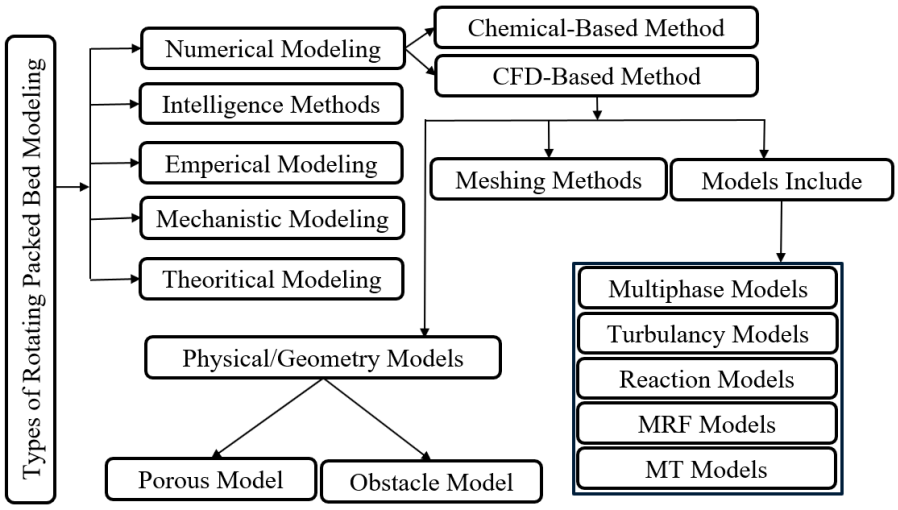

Figure 2. RPB modeling approaches.

3.1. Hydrodynamic Modeling

Hydrodynamics is the study of fluid motions [79] and includes pressure drop, flooding and liquid hold-up [79]. Basic and detailed experimental research is required for explaining hydrodynamics and MT in RPBs, as well as their correlations [80]. On the other hand, MT performance strongly depends on fluid flow patterns [66]. The hydrodynamic parameters employed for RPB scale-up and design [81], which are going to be reviewed in this section, are shown in Figure 3. Regarding these important issues, investigators have determined many correlations for three models—flooding, pressure drop and hold-up models—as described below.

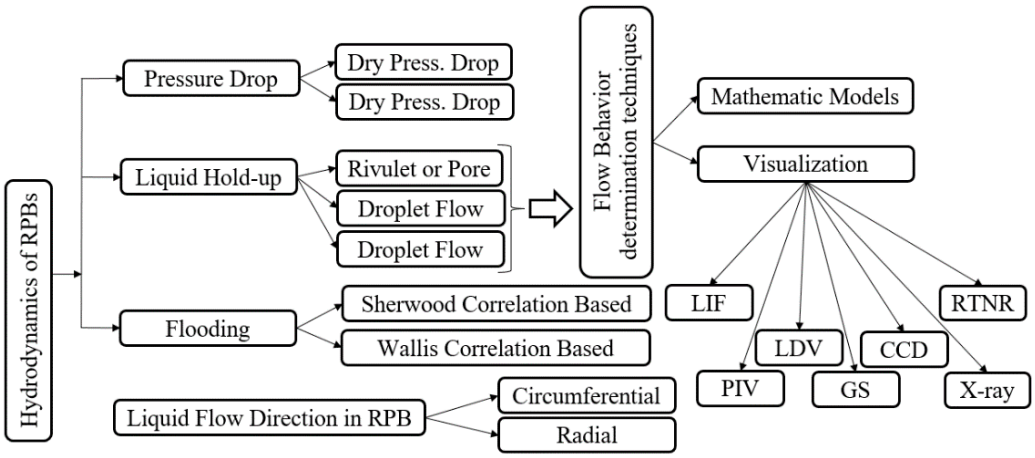

Figure 3. Approaches to the modeling of hydrodynamic parameters.

3.1.1. Liquid Behavior and Hold-Up

The liquid patterns in RPBs can be classified into the three categories of droplet flows, film flows and pore (thread or ligaments) flows, which were proposed by Burns and Ramshaw [82] following visual observation and photography, which confirmed the presence of pore and droplet pattern flows, as shown in Figure 4.

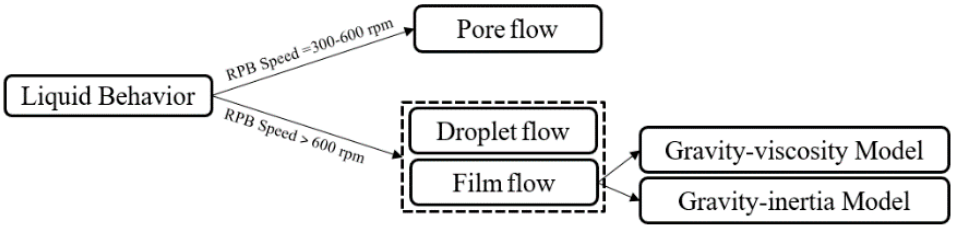

Figure 4. Liquid flow patterns in an RPB.

When the rotational speed is between 300 and 600 rpm, the pore flow regime is the dominant pattern in the RPB, wherin the liquid primarily flows in the form of radial rivulets, while the zones between them are empty, and this leads to a reduction in the MT effective surface area. When the rotational speed exeeds 600 rpm, the liquid's behavior changes to a droplet flow and then to a film flow pattern [27,82,83]. Generally speaking, centrifugal increments make film flows thinner and cause the mass fluxes to increase [84].

Generally, the most prominent visualization techniques for determining flow fields and behavior in packed beds include gamma scanning [85], tomography [86], X-ray [83], *PIV* measurement [87], *RTNR* [88], and *CCD* camera [89].

S. Munjal et al. illustrated that δ was affected by the liquid kinematic viscosity, flow rate, packing radius and annular speed of RPBs [30]. Later, researchers developed empirical correlations for predicting the thickness of liquid elements. A brief summary of these correlations, developed between 2000 and 2020, is given in Table 2, which confirms

the results of Manjal et al.'s study and illustrates that the liquid's properties, along with packing configuration and rotation rate, determine the amount of δ.

Some investigators applied the above findings in the hydrodynamic analysis of RPBs in their studies. X. Li et al. [90], for example, reported that when the acceleration was lower than 60 g in a rotating fin baffle packed bed contactor, the dominant regime was film flow, and that Guo et al.'s correlation could be used to calculate the thickness of the liquid film. This correlation, as shown in Table 2, demonstrates that liquid thickness reduces when the rotational speed increases.

Sang et al. [91] analyzed fluid patterns in RPBs with high-speed photography. They found that the liquid flow would take the form of ligaments, which exited the packing at lower rotational speeds (pore flow) and grew in numbers at higher speeds, then finally disappeared. Drawing on the results of their study, they categorized liquid patterns into ligament or pore flows and droplet flows, suggested six parameters that affect the flow regime, and proposed a criterion to determine the regime based on the relation between the Re and We numbers via the new dimensionless number of q, which is defined by the liquid's initial velocity, the annular speed, and the outer rotor diameter.

Additionally, Sang et al. reported that most of the MT in the cavity zone of their RPB was carried out by droplet collisions with the casing wall. They considered the deposition splashing of a liquid (droplets) using Ohnesorge and Reynolds numbers. They proposed a set of criteria relation criteria named "splash criteria", and reported that the MT in the cavity zone was due to droplet interaction with the inner wall of the casing [25].

Li et al. studied the liquid flow situation in an RPB with a charge-coupled device (*CCD*) camera [89]. They reported the non-continuity of film–ligament droplets at low velocities and weaker surface tension at higher velocities, showing that the liquid flow turned into droplets at higher velocities. Moreover, they argued that the break-up and coalescence of liquids may occur when droplets fly in RPBs, which is determined by

$$We = \frac{\rho_G \left|\vec{v_L} - \vec{v_G}\right|^2 D}{\sigma_L} > 12 \quad (1)$$

where Weber numbers lower than 12 indicate that liquid breaking occurred in the cavity zone. They proposed a correlation with a $\pm$15% error using

$$d = 5.03 \times N^{-0.347} u_0^{0.183} \quad (2)$$

Table 2. Estimation of liquid element thickness via empirical correlations.

Author	Year	RPB Type	Kind of Packing	Liquid Form	Correlation
Burns et al. [92]	2000		Glass sphere		$\overline{\delta} = 2.25\left(\frac{\nu_L u_L}{a_w a_c}\right)^{\frac{1}{3}} \overline{\delta} = 2.59 \frac{u_L}{a_w a_c^{\frac{1}{2}} d_{pore}^{\frac{1}{2}}} \left[\frac{1-(1-K)^{\frac{1}{2}}}{K^{\frac{1}{2}}}\right]$: Inertia flow $\overline{\delta} = 2.25\left(\frac{\nu_L u_L}{a_w a_c}\right)^{\frac{1}{3}}$: Viscos flow
C. C. Lin et al. [93]	2000		Glass sphere		$\delta = \frac{4Q_L d}{5\pi r u_{r,L} h}, \overline{\delta} = \frac{1}{R_o - R_i} \int_{R_i}^{R_o} \delta dr$
Chen et al. [33]	2003		Metal wire mesh		For complete wetted packing: $\overline{\delta} = 4106 u_{L,i}^{0.454} u_{G,i}^{-0.002} \omega^{-0.104}$ For partial wetted packing: $\overline{\delta} = 2055 u_{L,i}^{0.183} u_{G,i}^{0.003} \omega^{-0.109}$
Yi et al. [94]	2009		Wire mesh	Droplet	$d = [0.826 + 17.4(r - r_i)]d_1, r - r_i < 0.01$ m Cavity zone $d = 12.84\left(\frac{\sigma_L}{\omega^2 r \rho_L}\right)^{0.63} u_L^{0.201}$ Bulk zone
Li et al. [95]	2009			Film	$\delta = \left(\frac{3\nu_L Q}{r\omega^2}\right)^{\frac{1}{3}}$
Yang et al. [96]	2010			Droplet	$\overline{d} = C\left(\frac{\sigma}{\omega^2 r \rho_L}\right)^{0.5}$
Sang et al. [91]	2017				$\frac{d_{droplet}}{R_o} = 0.042 We^{-0.272} Re^{0.068} q^{0.098} \left(\frac{R_o}{R_{Rotor}}\right)^{-0.776}$ For cavity zone
Sang et al. [97]	2019	Simple			$d_e = [0.826 + 17.4(r_e - r_i)]d_1 d_{ez} = [0.826 + 17.4(r_{ez} - r_i)]d_1$ End-effect zone $d_b = 12.84\left(\frac{\sigma}{\rho_L r_b \omega^2}\right)^{0.630} u_{L,b}^{0.201} d_{bz} = 12.84\left(\frac{\sigma}{\rho_L r_{bz} \omega^2}\right)^{0.630} u_{L,bz}^{0.201}$ Bulk zone
Wang et al. [98]					$\overline{d_i} = 0.7284\left(\frac{\sigma_L}{\omega^2 R_p \rho_L}\right)^{0.5}$ Bulk zone $\frac{\overline{d_o}}{r_o} = 0.042 We_L^{-0.272} Re_L^{0.068} q_L^{0.098} \left(\frac{R_o}{R_i}\right)^{-0.776}$ Cavity zone $q_{L,0} = \frac{u_{L,0}}{\omega r}$
Su et al. [99]	2020		Metal wire mesh		$\frac{d_{avg}}{d_0} = 8.58 We^{-0.18} Re^{-0.24} N_p^{0.44} (1 - Cos\theta_{adv}^*)^{-0.12} \left(\frac{h_1}{h_{max}}\right)^{-0.18}$

Recently, Hacking et al. [100] examined several kinds of concentric redistribution rings in an RPB operated in the speed range of 500–1200 rpm, and reported that this type of liquid distribution could improve the uniformity of liquid distribution, thus increasing the wetting and effective surface areas and reducing the channeling area in the packing zone.

In PBCs, it is important to know the hold-up in order to determine the dynamics of the tower, because this affects the mass transfer and pressure drop. In addition, the hold-up directly affects the operating weight of PBCs and, therefore, the design of the supports [101]. The term "hold-up" describes the volume of liquid present on the surface of the packing in the form of a film or ligaments, or droplets in the voidage of the packing in the form of rivulets. There are two types of hold-up: static and dynamic (operating). The first term refers to the liquid inventory in the packing where gas and liquid do not flow, and the second one refers to the liquid inventory when both liquid and gas flow. The hold-up in random packing is defined by the summation of both (static and dynamic) the terms [102]. Most researchers report total hold-up, and do not establish this parameter separately in their correlations [102]. Hold-up estimation allows for the determination of residence time in the packing, and is especially important when the system contains a special mixture that is sensitive to temperature or reactive absorption processes [103]. There are many correlations available to help predict the liquid hold-up in PBCs [104,105], but because of the existence of radial flows in an RPB's geometry, the liquid hold-up equations for RPBs are not the same as those for PBCs. The rotational speed reduces the hold-up and simplifies the gas passage, as Lashkarbolooki [106] showed. Theoretically, the mean hold-up in RPBs may be defined by the following equations [93]:

$$\overline{h}_L = \frac{V_L}{V_B} \tag{3}$$

$$V_B = \pi\left(R_o^2 - R_i^2\right)Z \tag{4}$$

Other methods for hold-up measurement, such as gamma absorption [103], conductance measurement [107] and the neural network method [108], are empirical.

Basic and Dudukovic [107] defined a correlation, according to their empirical data, using Re and Ga numbers and packing characteristics. F. Guo et al. focused on cross-flow simple RPBs equipped with wire gauze packings, and determined the amount of hold-up by considering the ratio of the liquid area flow rate to the liquid mean radial velocity [27]. C. C. Lin et al. [93] developed a correlation via the theoretical analysis of liquid hold-up for a simple counter-current RPB based on one rotating disk. They modeled their work on the layers of hypothetical rotating disks, and verified their analysis with experimental pressure drop data. Considering the mean liquid film, they described the hold-up thickness as follows:

$$h_L = \overline{\delta} \times a_w \tag{5}$$

$$\overline{\delta} = \frac{1}{R_o - R_i}\int_{R_i}^{R_o} \delta dr \tag{6}$$

Finally, according to their experimental data, they proposed a prediction correlation to estimate the hold-up for co-current systems that used the modified Galileo number, Ga*.

In the same year, Burns et al. [92] reported that hold-up prediction for RPBs can be performed using the following equations for pore and droplet flows, respectively.

$$h_L = 1.41\frac{u_L}{a_c^{\frac{1}{2}} d_{pore}^{\frac{1}{2}}}\left[\frac{1-(1-K)^{\frac{1}{2}}}{K^{\frac{1}{2}}}\right],\ 0 < K < 1 \tag{7}$$

$$h_L = 1.41\frac{u_L}{a_c^{\frac{1}{2}} \overline{d}_{pore}^{\frac{1}{2}}} \tag{8}$$

They performed electrical resistance measurements to empirically determine the hold-up and residence time in RPBs with a kind of reticulated foam packing, and proposed the following general equations, which exclude the effects of gas flows on hold-up for propylene glycol and water, respectively.

$$h_L = 0.039\left(\frac{a_c}{a_0}\right)^{-0.5}\left(\frac{u_L}{u_0}\right)^{0.6}\left(\frac{\nu}{\nu_0}\right)^{0.22} \quad (9)$$

$$h_L = 0.034\left(\frac{a_c}{a_0}\right)^{-0.38}\left(\frac{u_L}{u_0}\right)^{0.62} \quad (10)$$

where

a_0: 100 m/s^2
u_0: 0.01 m/s
ν_0: 1CS or 10^{-6} m^2/s

They also highlighted that when $Re\bar{\delta} \gg d_{pore}$, an inertia flow is dominant, while when $Re\bar{\delta} \ll d_{pore}$, a viscose flow is dominant.

Later, Chen et al. [33] studied this subject, assuming that the gas and liquid took the form of plug and film flows in steel wire mesh RPBs, and derived a hold-up correlation with regression from their experimental data. They illustrated that hold-up could be determined via the initial superficial liquid and gas velocities, as well as the annular velocity.

For the accurate estimation of hold-up in RPBs, Yang et al. [83] used an X-ray CT scanner. Their analysis of the time-averaged tomographic photographs of the surface area showed that a high rotating speed improved liquid distribution in the packing. Their experimental results showed that the hold-up decreased with an increase in rotation. Finally, Yang et al. proposed the following correlation with a ±22% error by adding the Kapitza number, which included surface tension, to Basic and Dudukovic's correlations.

$$h_L = 12.159Re^{0.923}Ga^{-0.61}Ka^{-0.019} \text{ For wire mesh packing} \quad (11)$$

$$h_L = 12.159Re^{0.479}Ga^{-0.392}Ka^{-0.033} \text{ For nickel foam packing} \quad (12)$$

After that, Liu et al. [109] carried out the same study, and proposed correlations with a lower error (±15%) that were similar to those of Yang et al., and which were devised for an RPB that was equipped with a mesh-pin rotor.

$$h_{L,IMZ} = 5.835Re_L^{0.854}Ga^{-0.454}Ka^{0.037} h_{L,OPZ} = 0.247Re_L^{0.427}Ga^{-0.239}Ka^{0.031}$$

Another operating parameter in RPBs is the liquid residence time, which can be determined via liquid hold-up prediction [107]. K. Guo et al. [110] studied the residence time distribution (RTD) in an RPB with simple wire mesh screen packing. They reported that the average residence time was a function of the liquid flow rate and rotational speed, with a reverse relationship. Similarly, D. Xinlin et al. explained liquid mean residence time in a simple RPB based on a modified surface renewal model [111].

3.1.2. Flooding and Pressure Drop

Generally speaking, the flooding point is defined as the upper limit of a contactor's operation, its permissable flow rates, as well as the liquid and gas velocities at which high rates of pressure drop and low MT efficiency occur. The flooding point in PBCs is not exactly the same as that in RPBs because of the presence of centerifugal accerelation, the orientaion of the rotors, and the flow areas in RPBs. However, the flooding point in RPBs depends on the total pressure drop, as well as gas and liquid flow rates [84,112], and it does not allow operation at high throughputs. Sivakumar [113] also argued that high gravity limits flooding in RPBs, compared to PBCs, and establishes more effective gas–liquid surface areas in the packing. RPBs have a higher flooding capacity due to their

high gravity, as reported by Hendry et al. [81], who also showed how a flooding point could be determined and measured. Gas velocity and effective surface area increase as a result of an increase in acceleration, which can reduce the volume of the contactor. Greater centrifugal acceleration allows for greater flooding capacity [84,114]. Neumann et al. [114] examined knit meshes, metal foam, and two types of fixed nozzles (flat fan (FF) and full jet (FJ)), and reported that FF nozzles reduced the flooding point and that the effect of the packing type was tiny. Their experimental results indicate that the flooding point depends on gas capacity, liquid loads, rotational speeds, liquid distributor types, and packing characteristics.

A greater flooding capacity allows the use of high-volume of more porous packings. Furthermore, the flooding is locally affected, with the liquid hold-up from the inner to the outer edge decreasing and becoming thinner due to centrifugal acceleration and flow area increment. Therefore, selecting the most suitable liquid distributer can improve these aspects. Near the flooding point, a greater pressure drop and MT rate are achieved, after which the MT rate drops to a minimum and the *NTU* decreases when the operation reaches its flooding point [81,84,112,113,115].

There are two approaches to flooding prediction in PBCs. One method is based on generalized correlation charts for irrigated beds, known as GPDC (Generalized pressure drop correlation) charts, and the second method focuses on theoretical models for describing one or two phases in the column. With these approaches, famous correlations, such as those of Wallis and Sherwood, were established [116]. In the Sherwood approach, $\frac{u_G^2 a_t}{g\varepsilon^3}\left(\frac{\rho_G}{\rho_L}\right)^{0.2}\mu_L^{0.2}$ (Y axis) vs $\frac{L}{G}\left(\frac{\rho_G}{\rho_L}\right)^{0.5}$ (X axis) gives the flooding limitation [117], and in that of Wallis, two other parameters are used, the summation of which is one constant, as follows [118]:

$$C_G^{0.5} + mC_L^{0.5} = C \tag{13}$$

$$C_G = \frac{M_G}{\rho_G A}\left(\frac{\rho_G}{\rho_L - \rho_G}\right)^{0.5} \tag{14}$$

$$C_L = \frac{M_L}{\rho_L A}\left(\frac{\rho_L}{\rho_L - \rho_G}\right)^{0.5} \tag{15}$$

Furthermore, in 1992, Singh et al. proposed a modified Sherwood correlation in the following form, according to their RPB experimental data for a VOC removal system [119].

$$log\left[\frac{u_G^2 a_t}{R_i\omega^2\varepsilon^3}\left(\frac{\rho_G}{\rho_L}\right)\left(\frac{\mu_L}{\mu_w}\right)^{0.2}\right] = -2.27 - 1.14log\left(\frac{L}{G}\sqrt{\frac{\rho_G}{\rho_L}}\right) - 0.17\left[log\left(\frac{L}{G}\sqrt{\frac{\rho_G}{\rho_L}}\right)\right]^2 \tag{16}$$

They examined the hydraulic capacity of a simple counter-current RPB, and compared their experimental results with those of the Sherwood corrolation. The experimental data showed good compatibility with wire gauze packing, and they underestimated the ω for the Sumitomo packing. Kelleher and Fair [84] reported that the hydraulic capacity and area of the flows on the packing's inner surface could be predicted via the Sherwood method by replacing g with a_c for RPBs. Rao et al. [112] suggested that the term "ejection point" was a better expression than "flooding point", which denotes the point where at the pressure drop across the rotor increases with a reduction in the angular speed, and they made use of the Sherwood approach in their investigation of an RPB by replacing g with a_c. The experimental results of Wang et al.'s investigation [62] demonstrate that the hydraulic capacity is a function of vapor velocity at the eye of the rotor. Y. Li et al. [115] investigated an air–water system, and showed that the flooding point in *RZB*s and RPBs was that at which the pressure drop increased quickly when the superficial liquid velocity increased. They proposed a modified Sherwood correlation (17) for *RZB*s, without considering a_t and ε, as follows:

$$log\left[\frac{u_{G,\Delta r}^2}{R_i\omega^2\Delta r}\left(\frac{\rho_G}{\rho_L}\right)\right] = -2.281 - 0.9788log\left(\frac{L}{G}\sqrt{\frac{\rho_G}{\rho_L}}\right) - 0.1605\left[log\left(\frac{L}{G}\sqrt{\frac{\rho_G}{\rho_L}}\right)\right]^2 \quad (17)$$

where Δr is the distance between the inner rotational and stationary baffles.

Lockett [120] reported that the Wallis type plot was better than the Sherwood type for correlating flooding data in RPBs, and proposed a correlation based on the Wallis correlation that Rajan et al. [121] provided. This correlation, based on their experimental data for an *RSB*, is as follows:

$$C_G^{0.5} + mC_L^{0.5} = 1.57\beta^{0.25}a_t^{-0.25}\left(\frac{\mu_L}{\mu_w}\right)^{-0.03} \text{ Lockett's extended form} \quad (18)$$

$$C_G^{0.5} + 1.51C_L^{0.5} = 130\beta^{0.434}a_t^{-0.9343}\left(\frac{\mu_L}{\mu_w}\right)^{-0.03} \text{ Rajan et al.'s extended form} \quad (19)$$

$$C_G = u_G\left(\frac{\rho_G}{\rho_L - \rho_G}\right)^{0.5} \quad (20)$$

$$C_L = u_L\left(\frac{\rho_L}{\rho_L - \rho_G}\right)^{0.5} \quad (21)$$

Another important parameter is the minimum height for an RPB without flooding, which was defined by K. Gudena et al. [122] as Equation (22):

$$h_f = \frac{Q_G}{2\pi R_i u_g} \quad (22)$$

In addition, they applied Equation (23) to determine the minimum length of an RPB's inner radii.

$$r_{i,min} = \left(\frac{Q_G}{\pi u_{jet}(1 - f_d)}\right)^{1/2}\left(\frac{\rho_G\xi}{\rho_L}\right)^{1/4} \quad (23)$$

where the unit of Q_G is m^3/s.

The loss of momentum in RPBs due to fluid flow resistance across porous media causes a pressure drop in the whole packing [123], which can be computed using the various models and approaches developed by investigators. The measurement and calculation of the pressure drop in RPBs is more complicated than in PBCs. Additionally, a pressure drop in RPBs may be described as dry or wet by investigators. A dry pressure drop is determined when only gas flows across the RPB, while it is called a wet pressure drop when liquid and gas are introduced simultaneously.

In 1990, Kumar and Rao [124] proposed a correlation to evaluate the pressure drop for counter-current simple RPBs with wire mesh packing, and defined the total pressure via friction forces, centrifugal pressure drop, and increases in (rotating and translational) kinetic energy, as follows:

$$\Delta P_t = \Delta P_c + \Delta P_f + \Delta P_k \quad (24)$$

Singh et al. [119] evaluted RPBs with three kinds of rotor in the context of removing VOC from water, and proposed the following correlation, which only includes a pressure drop due to the rotaion and friction of fluid in the packing.

Foumeny et al. [125] investigated equilateral and non-equilateral solid cylinders as packing in a tube, and proposed an empirical correlation useful for pressure drop estimation that uses the size of particles and their relation to the bed diameter, thus resolving the deficiencies of Ergun's correlations. In the same year, Hwai-Shen Liu et al. evaluated the dry and wet pressure drop in a simple counter-current RPB using the gas capacity factor, as well as the wetted and dry resistance coefficients, which depend on Q_L, Q_G, and the annular velocity of the packing [28]. Additionally, their experimental results showed that,

due to the reduced liquid hold-up, the effects of Q_L were more significant in rectangular packing than in elliptical packing with different rotor speeds.

Rao et al. [112] contended that a dry pressure drop across the stationary rotors in simple RPBs can be predicted by the Ergun correlation, as follows:

$$\frac{dP}{dr}\frac{\varepsilon^3\rho_g d_p}{(1-\varepsilon)\dot{m}_g^2} = \frac{150(1-\varepsilon)}{Re_p} + 1.75 \tag{25}$$

and according to the flow area variations, they changed it to the following form:

$$\Delta P = \frac{(1-\varepsilon)}{\varepsilon^3}\frac{Q_g}{2\pi Z d_p}\left[\frac{150(1-\varepsilon)\mu_g}{d_p} ln\frac{R_o}{R_i} + 1.75\frac{Q_g\rho_g}{2\pi Z}\left(\frac{1}{R_i} - \frac{1}{R_o}\right)\right] \tag{26}$$

They reported that a dry pressure drop was induced linearly with a change in the rotor's speed, and that it initially decreased when liquid flowed in, while it remained constant when the speed was increased, which might have caused a reduction in the liquid hold-up [112]. In this experiment, the total pressure drop was defined in three segments across the RPB by Equation (24); Equation (26) was employed to determine the amount of ΔP_f, and Equations (27) and (28) were used to estimate the kinetic and centrifugal pressure drop.

$$\Delta P_k = \frac{\rho_g}{8}\left(\frac{Q_g}{\pi Z}\right)^2\left(\frac{1}{R_o^2} - \frac{1}{R_i^2}\right) \tag{27}$$

$$\Delta P_c = \frac{A}{2}\rho_g\omega^2\left(R_o^2 - R_i^2\right) \tag{28}$$

where A is a constant in the range of 0.5–2.

Chandra et al. [126] reported that gas velocity and rotor speed could increase the total pressure drop through rotors in an *RSB*. Wei-Der Sung and Yu-Shao Chen presented an RPB that was equipped with a blade and baffle. Their enforced modification baffle reduced the pressure drop by 53% [127]. Wang et al. [128] studied a cross-flow RPB with concentric ring packing (*CRB*), and suggested a correlation that could calculate the degree of pressure drop according to the gas and liquid's superficial velocities and rotational speeds. The experimental results of this investigation show that the degree of dry pressure drop did not vary with an increase in the gas velocity. Furthermore, the rotational speed had no effect on the dry pressure drop, but the degree of wet pressure drop increased with an increase in the rotational speed.

Although Lashkarbolooki [106] reported that the major parameters impacting simple RPBs' pressure drop rates were gas and liquid flow rates and rotor speeds, Neumann et al. [80] employed a channel model, and pointed out that the geometry of the packing was not considered in Ergun's correlation. They showed that the centrifugal pressure drop mainly depends on the outer radii of the rotors, and the friction pressure drop depends on the geometry of the rotors and the packing characteristics when under the operation conditions of RPBs.

Several of the pressure drop correlations proposed by investigators between 2009 and 2017 are summerized in Table 3. These correlations illustrate that the total pressure drop depends on the gas capacity factor, gas and liquid flow rates, the rotational speed of the packing, and gas density.

Table 3. Summary of several pressure drop correlations published by investigators between 2009 and 2017.

RPB Type	Year	Kind of Packing	Flows Contacting	Correlation	Div. (%)	Refs.
CRB	2009	Concentric ring	Cross-current	$\Delta P = 0.019 n^{0.35} Q_{s,L}^{0.018} u_g^{0.95}$, $u_g = \frac{4\dot{m}_g}{\rho_g \pi D_i^2}$, $Q_{s,L} = \frac{3600\dot{m}_g}{\pi R_i \rho_L h_c}$	±20	[128]
Simple	2009	Wire mesh	Counter-current	$-\Delta P_t = \Delta P_I + \Delta P_{II} + \Delta P_{III}$ $-\Delta P_I = \frac{\rho_G Q_G^2}{8\pi^2 Z_1^2}\left(\frac{1}{R_2^2 - R_1^2}\right) + \int_{R_2}^{R_1} \rho_G \frac{u_\theta^2}{r} dr$ $-\Delta P_{II} = \xi \frac{\rho_G}{2R_h}\left(\frac{Q_G}{8\pi\varepsilon r Z_2}\right)^2 \left(\frac{1}{R_3} - \frac{1}{R_2}\right) + \frac{\rho_G Q_G^2}{8\pi^2 Z_2^2 \varepsilon^2}\left(\frac{1}{R_2^3 - R_2^2}\right) + \int_{R_3}^{R_2} \rho_G \frac{u_{\theta II}^2}{r} dr$ $-\Delta P_{III} = \frac{\rho_G Q_G^2}{8\pi^2 Z_2^2}\left(\frac{1}{R_4^2 - R_2^3}\right) + \int_{R_3}^{R_4} \rho_G \frac{u_{\theta III}^2}{r} dr$	±5	[129]
Simple	2010	Plastic porous plate packing Rippled porous plate packing	Cross-current	$\Delta P_d = 0.06920 \beta^{0.6764} Q_G^{0.8203}$ $\Delta P_w = 0.08486 \beta^{0.519} Q_G^{0.8529} Q_L^{0.0945}$ $\Delta P_d = 0.1515 \beta^{0.5201} Q_G^{0.9117}$ $\Delta P_w = 0.07956 \beta^{0.4499} Q_G^{1.0387} Q_L^{0.0792}$	±10	[130]
RZB	2013	Stationary and rotating baffle	Counter-current	$\Delta P_D = \frac{1}{2}\rho_G \left(\frac{u_{G,avg}}{\varphi}\right)^2 \frac{f_d}{d_h}(r_o - r_i)$ $\Delta P_w = \frac{1}{2}\rho_G \left(\frac{u_{G,avg}}{\varphi}\right)^2 \frac{f_w}{d_h}(r_o - r_i)$ $f_d = (1.013 \times 10^7) Re_G^{-4.004} + 0.001942 Re_G^{-0.903} Re_\omega^{1.151}$ $f_w = 0.1159 Re_G^{-1.308} Re_L^{0.0384} Re_\omega^{0.936} + 3.819 Re_L^{-0.0331}$	4.02–12.38 3.20–11.32	[131]
Simple	2017	Wire mesh, Sumitomo, foam metal	Counter-current	$\Delta P_t = A\left(\frac{Q_G}{2\pi Z}\right) ln\left(\frac{R_o}{R_i}\right) + B\left(\frac{Q_G}{2\pi Z}\right)^2 \left(\frac{1}{R_i} - \frac{1}{R_o}\right) + \frac{\rho g}{2}(K\omega)^2 (R_o^2 - R_i^2) + (S_1 + S_2)(u_G - u_L)$	7.24	[106]
Simple	2017	Knit meshes and metal foams	Counter-current	$\Delta P_{tot} = A_{CH} \frac{\rho_G \omega^2}{2}(R_o^2 - R_i^2) + \Delta P_{f,sta} + \Delta P_{f,empty} + \Delta P_{f,rotor} + \Delta P_{rot}$ $\Delta P_{f,state} = \Psi_0 (1 - \varphi) \frac{1-\varepsilon}{\varepsilon^3} \frac{\overline{F}_{G,int}^2}{d_p} \frac{(R_o - R_i)}{K}$ $\overline{F}_{G,int} = \frac{\sqrt{\rho_G}}{R_o - R_i} \int_{R_i}^{R_o} u_G(r) dr = \frac{Q_G}{2\pi Z (R_o - R_i)} ln\left(\frac{R_o}{R_i}\right) \sqrt{\rho_G}$ $\Psi_0 = \frac{725.6}{\overline{Re}_{G,int}} - 3.203$, $\overline{Re}_{G,int} = \frac{d_p}{(1-\varepsilon)\nu_G} \frac{\overline{F}_{G,int}}{\sqrt{\rho_G}}$	±15	[80]

3.2. Mass Transfer and Performance Modeling

3.2.1. Mass Transfer Coefficients and Removal Efficiency

The mass transfer of soluble components depends on fluid motion in the field. The MT coefficient is a function of the fluid properties and flow rate, and will vary if these parameters cause any variations in the flow direction [132]. The MT rate can be affected by several parameters, such as the packing type, the absorbent physicochemical's properties and concentration, the absorbing component's partial pressure, gas flow rate, liquid flow rate, liquid temperature, and the loading of the components in the absorbents in PBCs [133]. The gas velocity and flow area change radially in RPBs; therefore, MT coefficients change from point to point in the contactor [134], but there is no general theory in this case, and the prediction of MT coefficients in RPBs is theoretically complicated [30]. The MT correlations developed by researchers for RPBs are theoretical or empirical correlations, and some of them replace the term "g" with "$r\omega^2$" so as to use the conventional PBC correlations. For instance, H. H. Tung and R. S.H. Mah developed a theoretical equation for penetration theory, and showed that it could be made applicable for HiGee processes by replacing "g" with "$r\omega^2$" [135].

$$\frac{k_L d_p}{D_L} = \frac{2 \times 3^{0.33}}{\pi} Sc_L^{0.5} Re_L^{0.33} \left(\frac{a_t}{a_e}\right)^{0.33} \left(\frac{d_p^3 \rho_L^2 g}{\mu_L^2}\right)^{0.167} \tag{29}$$

Kang et al. [136] examined a CO_2–*MEA* system in an RPB by employing the two-film theory for mass transfer determination. Similarly, Joel et al. [137] worked on a CO_2–*MEA* system in 2015, and employed previous researchers' correlations for PBCs. Both of these replaced "g" with "$r\omega^2$" to use the correlations for RPBs. However, E. Oko et al. [138] demonstrated that estimating the gas–liquid effective interfacial area with the above method led to a noticeable error of around 50%.

The mathematical modeling of packed beds requires a system derived from heat, mass, and momentum conservation [139]. Reddy et al. [134] employed Equations (30) and (31) in the context of mass and energy balance to predict the overall gas volumetric MT coefficient, $k_G a$, in SO_2–NaOH systems, and the overall liquid volumetric MT coefficient, $k_L a$, when stripping oxygen from water for an *RSB*, as:

$$k_G a = \frac{Q_G}{\pi\left(R_o^2 - R_i^2\right) Z} ln \frac{C_{G,i}}{C_{G,o}} \tag{30}$$

$$k_L a = \frac{Q_L}{\pi\left(R_o^2 - R_i^2\right) Z} ln \frac{C_{L,i}}{C_{L,o}} \tag{31}$$

Yu et al. [140] applied Equation (30) in a simple RPB to predict $k_G a$ and Equation (32) to calculate *HTU* in CO_2 removal with a mixture of *PZ*-DEG.

$$HTU = \frac{R_o - R_i}{ln\left(\frac{Y_i}{Y_o}\right)} \tag{32}$$

According to this approach, Yu et al. [141] assumed an RPB in the form of several stirred tanks in series-mode and used a mole balance. Chu et al. [142] worked on SO_2–Na_2SO_3 systems, and similarly, Liangliang et al. [143] worked on SO_2 capturing with a calcium-based solution. Zhan et al. [144] studied the simultaneous absorption of H_2S and CO_2 into an M*DEA-PZ* solution in a simple RPB, and employed theoretical Equation (30).

Additionally, empirical and statistical correlations have been developed by investigators to enhance the accuracy and to identify more effective parameters. Munjal et al. [30] devised the following equations based on laminar liquid film flow to predict the liquid MT coefficient:

$$k_L = 2.6 \left(\frac{Q_L}{\Delta x}\right) Sc_L{}^{\frac{-1}{2}} Re_L^{\frac{-2}{3}} Gr_{av}^{\frac{1}{6}} \tag{33}$$

where $\Delta X = \frac{d_p}{2}$ is employed with higher liquid Reynolds numbers and $\Delta X = d_p$ with lower ones.

Liu et al. [28] and Chen and Liu [145] evaluated MT coefficients experimentally with gas and liquid Reynolds and Grashoff numbers, gas diffusivity, total packing surface area, and effective packing surface area.

Lin et al. [146] examined CO_2 absorption with NaOH, *MEA*, *AMP*, and *MEA-AMP* solutions in a simple RPB, reported the separation efficiency, and argued that $K_G a$ was a function of the rotational speed, absorbent concentration, CO_2 concentration, and gas and liquid flow rates. Chen et al. studied the effects of RPB geometry using different radius values of packing, and estimated the $k_L a$ according to their experimental results for the Sc, Re, Gr, and We numbers of liquid flow and packing characteristics [147]. Additionally, they reported that MT decreased with an increase in the outer radius of the packing at low rotational speeds, and that this decrease was small at high rotational speeds. Similarly, Chen et al. [148] evaluated MT for various types of structured and random packing (beads, Rashing rings, Intalox Saddles and wire meshes) at greater detail, considering packing characteristics such as the size, material shape, surface property, and fluid surface tension.

Yi et al. [94] worked on carbon dioxide capturing with a *DEA*-promoted hot potassium carbonate solution in a simple RPB, and demonstrated that the $K_G a$ in the end-effect zone was higher than in the bulk zone of the packing. They employed Onda et al.'s correlation (34) for PBCs.

$$\frac{k_G RT}{a_t D_G} = 2 \times Re_G^{0.7} Sc_G^{0.33} \left(a_t d_p\right)^{-2.0} \quad (34)$$

Equation (34) shows the co-rotation and counter-rotation modes and describes the volumetric liquid MT coefficient using liquid Reynolds, Froude, and Schmidt numbers, liquid diffusivity, total packing surface area, and equivalent diameter. A higher $k_L a$ was achieved using counter-rotation. Moreover, the liquid and gas' superficial velocities and centrifugal acceleration were changed radially in RPBs, and the *Re*, *Fr*, and *We* numbers were functions of the liquid's superficial velocity. In addition, the Fr and *We* changed with the centrifugal acceleration and packing surface area, respectively.

Lin and Chu [60] worked on a CO_2–NaOH system in a blade-type RPB, and their experimental data indicate that the carbon dioxide removal efficiency increased with the rotational speed, solvent flow rate, and concentration. Chen et al. [149] studied CO_2–NaOH and O_2 desorption from water in an RPB with two kinds of packing (plain-woven packing and knit-woven packing), and reported that RPBs with dense wire meshes would show reduced k_L and surface renewal due to their high resistance against flows. Their experimental results indicate that the a_e would be higher with stainless steel than with PTFE. They established a correlation by considering the shape parameter φ in addition to the Reynolds, Froude and Weber numbers, the surface property, the fluid surface tension, the gas diffusivity, and the equivalent diameter of the packing.

Recently, Chen et al. [150] worked on simultaneous NO_x–SO_2–CO_2 removal in a simple RPB, and proposed correlations based on the two-film theory, using the total surface area, gas diffusivity, equivalent diameter of packing, and the Reynolds, Froude, and Grashof numbers to estimate the gaseous volumetric MT coefficients, which increase with Fr reduction and increase with Re and Gr.

Another approach to MT prediction was proposed by Luo et al. [151], who contended that MT could be evaluated by dividing an RPB into three sections, namely, the bulk (packing), the cavity, and the end zone. This approach was proposed in Guo's dissertation, in which he argued that the liquid volumetric MT coefficients were highest in the end-effect zone, second highest in the bulk zone, and lowest in the cavity zone, but in industrial applications, the evaluation of MT in the bulk zone is more important than that in the other zones. It is assumed that the MT in the end-effect zone was related to the intense contact between the liquid elements and the packing, the strong interaction between gas and liquid, and the fast outlet of fresh liquid from the liquid distributor.

Yang et al. [152] reported that the MT in the cavity zone was 13–25% of the overall MT in the whole RPB. The experimental results of Guo et al.'s investigation [153] illustrate that the effective interfacial gas–liquid surface area in the cavity zone was approximately 30% of that of the whole RPB, and the residual value in the bulk zone was 70%. Sang et al. [25] investigated this issue in detail with a high-speed camera in a NaOH–CO_2 system, and analyzed the MT interfacial area in the cavity zone by considering the liquid elements as mother and daughter droplets and a liquid film. In the same year, the experimental result of Luo et al.'s investigation [154] demonstrated that the MT effective interfacial area in the cavity zone was about 9% of the whole interfacial area in their RPB.

In conclusion, correlations may be found via statistical regression analysis and dimensional analysis. A summary of the correlations developed by investigators in 2002–2019 to predict MT coefficients is given in Table 4. This table indicates that K_G, K_L, k_G, and k_L are functions of dimensionless numbers, which are expressed in terms of factors and variables depending on the system's behavior, as follows:

$$K_G = g(Re_G,\ Fr_G, Re_L, We_L, Fr_L, Ga, N, pH, C_{solvent}) \tag{35}$$

$$k_G a = h\left(Re_G, Re_L,\ Gr_G,\ Sc_G, \left(\frac{a_t D_G}{d_p}\right), Ga, We\right) \tag{36}$$

$$k_L a = I\left(Re_L,\ Gr_L,\ Sc_L, \left(\frac{a_t D_G}{d_p}\right), Fr_L, We_L,\ Re_G, Gr_G,\ Sc_G\right) \tag{37}$$

Additionally, as the table clearly shows, researchers have described the geometry of the system, the fluid's viscosity, and the effects of external forces such as the turbulence of the fluid flow (resulting from the packing and RPB geometry), the liquid surface tension, and the effect of rotational speed (using the Re, We and Gr numbers, respectively), to evaluate the performance of the contactor and determine the volumetric MT coefficient. Furthermore, it is possible to scale up this correlation and achieve dynamic similarity by adding the Fr number. Further details are provided in Section 4.

Table 4. MT correlations proposed by various investigators for RPBs in 2002–2019.

Type of RPB	Absorbent	Absorbing Component	MT Correlations	Div.%	Year	Refs.
CCSR	—	O_2 desorption	$\frac{k_L a d_p}{D_L a_t} = 0.478 Re_L^{0.906} Gr_L^{0.275}$	±10	2002	[155]
CCSR	Water	VOC	$\frac{k_G a He^{0.27}}{D_G a_t^2} = 0.077 Re_G^{0.323} Re_L^{0.328} Gr_G^{0.18}$	±30	2002	[145]
CCSR	Water	VOC	$\frac{k_G a He^{0.315}}{D_G a_t^2} = 0.061 Re_G^{0.712} Re_L^{0.507} Gr_G^{0.326}$	±30	2004	[156]
CCSR	—	O_2 desorption	$\frac{k_L a d_p}{D_L a_t} = 0.9 Sc_L^{0.5} Re_L^{0.24} Gr_L^{0.29} We_L^{0.29}$	±30	2005	[157]
CCSR	—	O_2 desorption	$\frac{k_L a d_p}{D_L a_t}\left(1 - 0.93\frac{V_{Packing}}{V_{RPB}} - 1.13\frac{V_i}{V_t}\right) = 0.65 Sc_L^{0.5} Re_L^{0.17} Gr_L^{0.3} We_L^{0.3}$	±30	2005	[147]
RSB	NaOH	SO_2	For co-rotation: $k_G a = \left(7.62 \times 10^{-3}\right) Re_G^{0.832} Gr_G^{0.194} Sc_G^{1/3}\left(\frac{a_t D_G}{d_p}\right)$ $k_L a = 0.152 Re_L^{0.569} Gr_L^{0.140} Sc_L^{1/2}\left(\frac{a_t D_L}{d_p}\right)$ For counter-rotation $k_G a = \left(7.62 \times 10^{-3}\right) Re_G^{0.976} Gr_G^{0.132} Sc_G^{1/3}\left(\frac{a_t D_G}{d_p}\right)$ $k_L a = 0.152 Re_L^{0.48} Gr_L^{0.128} Sc_L^{1/2}\left(\frac{a_t D_L}{d_p}\right)$	±20	2006	[134]
Blade	Water	*IPA*	$\frac{K_G a d_p}{D_G a_t} = 0.027 Re_G^{0.679} Re_L^{0.245} Gr_G^{0.14}$	±10	2007	[155]
CRCSR	NaOH	CO_2	$K_L a = 0.003689 Re_G^{0.5449} We_L^{0.5476} Ga^{0.3428}$ Plastic porous plate $K_L a = 0.003968 Re_G^{0.1399} We_L^{0.4336} Ga^{0.2724}$ Steal rippled porous plate	±10	2010	[130]
CCSR	Water	Ammonia and VOC	$\frac{k_G a}{D_G a_t^2}\left(1 - 0.9\frac{V_{Packing}}{V_{RPB}}\right) = 0.023 Re_G^{1.13} Re_L^{0.14} Gr_G^{0.31} We_L^{0.07}\left(\frac{a_t}{a_p}\right)^{1.4}$	±30	2011	[158]
COCSR	NH_3 based sol.	SO_2	$K_G a = 0.08 Q_G^{-0.01} Q_L^{0.56} N^{0.36} pH^{0.57} C_t^{-0.76} C_{SO2}^{-0.09}$	±8	2014	[39]
CCSR	A.S	SO_2	$K_G a = 2.6 \times 10^{-4} Re_G^{0.60} Fr_G^{0.34} Ga^{0.47}$ SiC structured packing $K_G a = 2.7 \times 10^{-5} Re_G^{0.77} Fr_G^{0.21} Ga^{0.26}$ Plastic structured packing	±5 ±10	2015	[159]

Table 4. *Cont.*

Type of RPB	Absorbent	Absorbing Component	MT Correlations	Div.%	Year	Refs.
CRCSR	NaOH	CO_2	$k_L a = 1.8221\left(\frac{a_t D_L}{d_p}\right) Re_L^{0.6371} Gr_L^{0.0548} Sc_L^{0.0623}$	±10	2015	[160]
CCSR	*TEG*	H_2O	$\frac{K_G a d^2}{D_G \rho_G} = 0.1697\left(\frac{Y_w}{1-W_{TEG}}\right)^{0.231}\left(\frac{Q_G}{Q_L}\right)^{-0.236} Sc_G^{0.333} Re_G^{1.614} \lambda^{0.125}$	±20	2018	[161]
CCSR	NaOH	SO_2	$\frac{K_G a d}{D_G a_s} = 0.456 Re_L^{0.59} Re_G^{0.63} We_L^{0.07} Fr_L^{-0.06}\left(\frac{\sigma}{\sigma_c}\right)^{0.1}$	±20	2018	[162]
CCSR	Na_2SO_3	SO_2	$K_G a = 2.76 \times 10^{-5} Q_G^{0.22} Q_L^{0.43} N^{0.55} pH^{2.27} C_{Solvent}^{0.1}$	±15	2018	[142]
COCSR	NaClO	VOC	$K_G a = 8.5173\left(\frac{Q_L}{Q_G}\right)^{1.2357} \omega^{-0.2783} t^{-1.2783} pH^{-0.2351} C_{NaClO}^{0.0346}$	±30	2018	[163]
CCSR	*MEA*	CO_2	$k_G = 2a_t D_G Re_G^{0.7} Sc_G^{\frac{1}{2}} (a_t d_p)^{-2}$ Bulk and end-effect zone $k_G = \frac{D_G}{d}(2 + 0.552 Re_G^{0.5} Sc_G^{0.5})$ Cavity zone	±20	2019	[97]

A.S: ammonia-based solution; PWP: Plain-woven packing; KWP: knit-woven packing; CCSR: counter-current simple RPB; COCSR: co-current simple RPB; CRCSR: cross-current simple RPB.

3.2.2. Effective Interfacial Surface Area and Performance

The effective gas–liquid interfacial surface area of a contactor is central to absorption systems and depends on system characteristics [152]. The effective surface area in bubble absorbers is equivalent to the wet and total contacting surface areas, while, in PBCs, the effective surface area of the packing may be smaller than the wetted surface area in small packings with very high loadings [164]. The effective interfacial surface area in contactors is highly dependent on hydrodynamics [165]—with highly turbulent flows and super-high gravity, a thinner liquid film and finer droplets are produced, which enhances the gas–liquid surface area and MT. This was demonstrated through Liu et al.'s experimental results regarding the absorption of ozone into water in counter-current RPBs [166], and through the results of Liangliang et al.'s investigation [143] of the absorption of SO_2 in RPBs with plastic and metal packings. Therefore, effective liquid distribution can be considered as essential to achieving a higher value of MT.

The method for the determination of effective gas–liquid interfacial surface area is shown in Figure 5. Due to the lack of physical methods and their complexity when employed in RPBs to predict the value of a_e, chemical methods have often been applied by investigators, using the known kinetics of the reaction along with absorption theory. Examples of this include Munjal et al.'s investigation [31] with simple RPBs, Yang et al.'s study [152] of a simple RPB with various radii of packing, and Rajan et al.'s experiments [121] on *RSB*s. All of these researchers used NaOH–CO_2–N_2 systems in RPBs with a pseudo first-order reaction, and applied the Danckwerts model and Henry's law to define the absorption flux and total gas–liquid interfacial area; they then determined the effective interfacial surface area by dividing the result by the overall volume of the packing. Similarly, Luo et al. [151,167] used this method in an RPB with simple wire mesh and blade packing, and defined the pseudo first-order reaction as follows:

$$R_{CO_2} = k_L a_e C_{CO_2,L} \sqrt{1 + \frac{D_{CO_2} k_2 C_{NaOH,L}}{k_L^2}} = k_L a_e C_{CO_2,L} \sqrt{1 + M} \tag{38}$$

When $M \gg 1$, then

$$a_e = \frac{R_{CO_2}}{C_{CO_2,L} \sqrt{D_{CO_2} k_2 C_{NaOH,L}}} \tag{39}$$

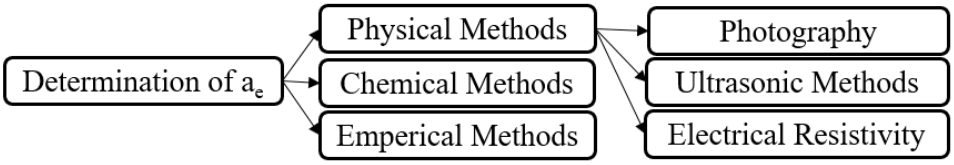

Figure 5. Effective interfacial surface area determination methods.

In the same situation, Dong et al. [160] applied the following equation for a simple cross-flow RPB.

$$a_e = \frac{R_{CO_2}}{H_{CO_2} p_{CO_2,L} \sqrt{D_{CO_2} k_1}} \tag{40}$$

Similarly, Tsai and Chen used a chemical method with a NaOH–CO_2 system in their RPB, which was equipped with blades and baffles, and proposed the following relationship for the CO_2 absorption flux (mol/m^2·s) [29]:

$$N_{CO_2} = \sqrt{D_{CO_2} k_1} a C^*_{CO_2} \pi \left(R_o^2 - R_i^2 \right) Z \tag{41}$$

wherein the rate constant of the pseudo first-order reaction is k_1.

Generally, in PBCs, it is assumed that the gas–liquid interfacial area is the same as the wetted surface area of the packing. In 1968, Ondea et al. [168] proposed an empirical correlation with a discripancy of ±20% to express the ratio of the effective interfacial area in the following form (basing this assumption on their experimental data for PBCs with four packing types):

$$\frac{a_e}{a_t} = 1 - exp\left[-1.45\left(\frac{\sigma_c}{\sigma}\right)^{0.75} Re^{0.1} Fr^{-0.05} We^{0.2}\right] \quad (42)$$

Similarly, Puranik and Vogelpohl [169] published the following emperical corrolation with a ±20% error:

$$\frac{a_e}{a_t} = 1.045 Re^{0.041} We^{0.133} \left(\frac{\sigma}{\sigma_c}\right)^{-0.182} \quad (43)$$

In high-gravity and -turbulance situations, the liquid layers are thinner and the droplets are finer, which gives rise to a wider contacting surface area and an intensified MT rate [143,166]. Lin et al. [93] developed the following correlation for an RPB with a maximum error of ±20%:

$$\frac{a_w}{a_t} = 584 Re_L^{-1.03} We_L^{0.576} Fr_L^{0.23} \quad (44)$$

Luo et al. [167] examined the effective interfacial surface area in an RPB with stainless steel wire mesh packing, and obtained an empirical correlation in a CO_2–NaOH system similar to that in Equation (44), with the addition of the shape factor to increase the accuracy of the system.

Xie et al. [170] proposed a correlation via the regression of 31 sets of CFD simulation data for RPBs with real 3D packings, with an error value of ±20%, as follows:

$$a_e = 202.3485\left(\frac{a_c}{205.6}\right)^{0.0435}\left(\frac{u_L}{0.0106}\right)^{0.4275}\left(\frac{\nu_L}{3.35}\right)^{0.1200}\left(\frac{\gamma}{75}\right)^{-0.5856} \quad (45)$$

Yan-Zhen Lu et al. [171] used surface-modified stainless steel wire mesh (SSM) and non-surface modified stainless steel wire mesh (NSM) in a simple counter-current RPB with an NaOH–CO_2 system, and their experimental results demonstrate that suitable liquid dispersion increased the a_e.

Other empirical correlations for gas–liquid interfacial surface areas developed by other researchers are shown in Table 5.

Table 5. Empirical correlations proposed by investigators for the prediction of effective surface areas.

Author	Year	RPB type	Packing	System	Correlation	Div. %
Rajan et al. [121]	2011	RSB	MF	NaOH-CO_2	$\left(\frac{a_e}{a_t}\right) = 54999 Re_L^{-2.2186} Fr_L^{-0.1748} We_L^{1.316}$: for co-rotation $\left(\frac{a_e}{a_t}\right) = 11906 Re_L^{-1.8070} Fr_L^{-0.0601} We_L^{0.9896}$: for counter-rotation	±15
Dong et al. [160]	2015	Simple	SSWM		$\frac{a_e}{a_t} = 2980.9 Re_L^{0.2349} Fr_L^{-0.045} Wr_L^{0.5023} \varphi^{-0.5}$	±10
Chen et al. [149]	2016	Simple	PTFE WM		$\frac{a}{a_t} = 11.057 Re_L^{0.359} We^{0.448} Fr^{-0.224} \varphi^{-0.202} \left(\frac{\sigma}{\sigma_c}\right)^{1.099}$: for PWP $\frac{a}{a_t} = 21.558 Re_L^{0.283} We^{0.317} Fr^{-0.218} \varphi^{-0.748} \left(\frac{\sigma}{\sigma_c}\right)^{1.099}$: for KWP	±20
Luo et al. [154]	2017	CCSR	SSWM		$\frac{a_e}{a_t} = 15.17 Re_G^{0.16} Re_L^{-0.38} Fr_L^{-0.13} Wr_L^{0.45} \varphi^{-0.29}$	±15
Xie et al. [170]	2019	Simple	Expanded SS mesh	*MEA*	$\frac{a_e}{a_t} = 202.3485 \left(\frac{a_c}{205.6}\right)^{0.0435} \left(\frac{u_0}{0.0106}\right)^{0.4275} \left(\frac{v}{3.35}\right)^{0.12} \left(\frac{\gamma}{75}\right)^{-0.29}$	±20

KWP: knit-woven packing; MF: metal foam; PWP: plain-woven packing; PTFE: polytetrafluoroethylene; SS: stainless steel; WM: wire mesh.

Additionally, three methods are available to evaluate the MT performance of a PBC, namely, evaluating the height of a transfer unit (*HTU*), evaluating the height equivalent to a theoretical plate (*HETP*), and evaluating the overall gas phase transfer unit. The main difference between a PBC and a HigGee is the height of the transfer unit (*HTU*) [84,165]. S. P. Singh et al. proposed Equation (46) to predict the area of the transfer unit (*ATU*) in counter-current simple RPBs [118].

$$ATU = \frac{\left(\frac{3.4\times10^4}{a_t^2}\right)\left(\frac{Q_L}{\mu_L a_t}\right)^{0.6}}{\left(\frac{\rho_L^2 g}{\mu_L^2 a_t^3}\right)^{0.15}} \quad (46)$$

T. Kellehr and J. R. Fair [84] reported that the value of *NTU* could be increased by raising the rotaional speed, and that a higher-pressure operation requires a higher *NTU*. It has also been argued that the MT performance may be measured via the size of the packing (R_o-R_i) and the *NTU*, which reveal the separation efficiency of a simple counter-current RPB. Gue et al. reported that the *HTU* could be defined as follows for a simple RPB [27]:

$$HTU = \frac{Q_L}{\pi K_L a\left(R_i^2 - R_o^2\right)} \quad (47)$$

where $K_L a$ is the liquid phase volumetric MT coefficent (mol/m^3·s), and Q_L is the liquid flow rate (m^3/m^{2}s).

C. C. Lin et al. [146] studied CO_2 absorption with NaOH, *MEA*, and *AMP*, and showed that another important parameter was the *NTU*, which could be evaluated by considering the mole fraction of CO_2 in the gas streams of the inlet and the outlet of an RPB. They suggested the following equation:

$$NTU = \int_{Y_o}^{Y_i} \frac{1}{Y - Y^*} dY \quad (48)$$

where they assumed that Y^* equals zero due to the fast reaction of CO_2 with the absorbing aqueous solution, and they proposed the following MT coefficient:

$$K_G a = \frac{Q_G(NTU_G)}{h\pi\left(R_o^2 - R_i^2\right)} = \frac{Q_G}{h\pi\left(R_o^2 - R_i^2\right)} ln\left(\frac{Y_i}{Y_o}\right) \quad (49)$$

D. P. Rao et al.'s investigation showed that the reduction in *HTU* in their simple RPBs was 5–10 times greater than that in conventional columns, and reported that the *HTU* did not change with angular velocity when MT-resistant control was enforced on the gas [113].

Additionally, G. Q. Wang et al. employed Equation (50) for the determination of *HETP* values in an *RZB* contactor [62]:

$$HETP = \frac{d_o - d_i}{N_T} \quad (50)$$

In 2009, Hsu-Hsiang Cheng and Chung-Sung Tan [37] applied Equation (51) to determine the *HTU* for CO_2 removal with blended alkanolamines as part of their evaluation of centrifugal acceleration and a fast reaction in a simple counter-current RPB equipped with stainless wire mesh packing.

$$HTU = \frac{R_o - R_i}{ln\left(\frac{C_{i,CO_2}}{C_{o,CO_2}}\right)} \quad (51)$$

C. H. Yu et al. examined CO_2 removal systems with aqueous and non-aqueous absorbents in a simple counter-current RPB, and showed that *HTU* would be reduced when

the rotating speed increased, and would increase with the gas flow rate [140]. Sheng et al. defined the *HTU* via the *NTU* in a simple counter-current RPB using Equation (52) [172]:

$$HTU = \frac{R_o - R_i}{NTU} \quad (52)$$

3.3. Numerical Methods

The numerical methods for analyzing RPBs are generally divided into two groups: chemistry-based (chemisorption) and CFD-based [72]. The chemistry-based methods are related to reaction kinetics and the above-mentioned correlations for mass transfer, while the other type is based on CFD models, which are described below.

CFD is an interdisciplinary topic that can be used to simulate flow characteristics and transport phenomena under certain conditions, and which includes mathematics, hydrodynamics, the computation of the conservation of mass, heat and momentum equations, and a discretizing method [173]. The velocity field in RPBs must be studied in order to determine heat and MT mechanisms, but the conditions in RPBs are complicated, turbulent, swirling and anisotropic [89], and CFD is a good tool in such situations. To improve the RPB's efficiency and flow, numerous researchers have focused on the CFD as related to hydrodynamic parameters, which include pressure drop and flow analysis. CFD modeling includes geometry definition, a meshing method, and models (multiphase, turbulence, and moving reference frame), as shown in Figure 2. Sometimes CFD modeling requires user-defined functions (UDF) for explaining reactions or MT. As for geometry generation, one of the following methods may be employed [173]:

1. Obstacle simplification (use of a simple geometry model or a representative elementary unit (REU), as used in [170];
2. Porous areas (use of mathematical methods that include viscosity and inertia resistance, which appear as a source term in momentum equations), which are suitable for RPB simulation on pilot and industrial scales;
3. Innovative models, such as Lu et al.'s [174], in which porous media are described based on the Kolodziej model, and that contained in another of Liu et al.'s investigations, wherein a physical model was defined via computed tomography (CT) reconstruction [175].

Yu-Cheng Yang et al. [173] reviewed the trends in CFD methods used to characterize an RPB, and concluded that obstacle simplification was a good approach for determining the liquid behavior, but it was not suitable for the 3D, pilot, or industrial scales, whereat porous media could be used.

One of the most important stages in RPB simulation is multiphase model selection. There are two major methods available for this goal: Euler–Lagrange and Euler–Euler, the second of which is widely used, and includes the volume of fluid (*VOF*), mixed, and Eulerian models [173]. The *VOF* model is not suitable for two- or three-dimensional (2D or 3D) pilot studies, while the Eulerian model, when used along with porous media models, is a good alternative, although it has been less commonly applied by investigators than the *VOF* model [66]. As regards the rotation of RPBs, it is necessary to define this situation with the multiple reference frame (MRF) or sliding mesh (SM) model [173]. H. Llerena-Chavez and F. Larachi applied the 3D physical unsteady-state model to simulate the air flow in a simple RPB, and applied porous media to define the packing. They validated the developed model with the experimental results of three RPBs [129]. Similarly, Wenjing Yang et al. [176] simulated the fluid flow in RPBs by applying 2D and 3D models to analyze the velocity profile in the bed. It was demonstrated that the effect of the packing rotation on the flow pattern was lower at a low inlet velocity. Martinez et al. [177] simulated multiphase flow behavior in a 3D model, which consisted of a water–sulfur dioxide system, and investigated the effect of the rotor speed on the flow pattern in an RPB. They considered the porous media in packed beds, which must be added as a momentum source term into standard fluid flow equations, and derived the same results for the gas inlet situation.

There is no general turbulent model for the simulation of RPBs. There are various models, which are categorized into the following two major approaches [173]:

1. Eddy viscosity models;
2. Reynolds stress transport models (RSM).

The RSM has a greater ability to give accurate predictions of complex flows, while five and seven additional equations, respectively, are required for 2D and 3D flows, which implies an increase in the calculation time and computational memory [173]. As such, the second group of models requires more time and computational memory, and is less attractive for researchers. Xin Shi et al. further developed this subject by studying the liquid droplet size and effect, size distribution, hold-up, and the effect of modifying the intensification of MT. They applied a 2D *VOF* model, a sliding mesh model, and an RSM in fluent solvers to simulate the velocity and liquid volume distribution, and concluded that the *VOF* model was suitable for defining the gas–liquid interface in RPBs [178]. A two-phase flow in an RPB was simulated with a 2D model, and the RNG k-ε and large discrete phase model (DPM) were selected by Cheng et al. as turbulence models for the continuous gas phase and liquid size distribution analyses, respectively [179]. They implemented a moving reference frame (MRF) of the packing area for the rotational section, and considered the following methods to compute the droplets' breakup:

1. Taylor analogy breakup (TAB) for $We < 100$;
2. Wave model for $We > 100$.

They reported that the value of the Weber number of the droplets increased in a radial direction, and that increasing the gas flow rate and rotor speed would increase the merging or breaking up of droplets in the packing. Yongli Sun et al. [180] simulated an *RZB* using a 3D model to analyze the pressure distribution and the optimal sizing of the packing. Yucheng Yang et al. studied the MT phenomena in a simple RPB. They developed a UDF solver in the Fluent software and adopted *VOF* and RSM models to simulate the multiphase flows in three different rotors [181]. Similarly, in the same year, Xue-Ying Gao et al. [182] worked on MT characterization for a simple RPB with a CO_2–NaOH system, using numerical simulation. They proposed a mathematical model that incorporated diffusion and reaction. Yi Liu et al. [183] developed a 3D physical model that used realizable k-ε, applied MRF models to simulate a simple RPB in a steady-state mode, and evaluated the air flow inside the packing and the pressure profile at various rotational speeds and gas flow rates. Additionally, Li et al. [89] employed an air–water system and studied the flow field in a perforated-ring RPB with a 2D obstacle physical model, using the RSM turbulence model. They defined air as the first phase and water as the second phase in a *VOF* model. They also used a *PIV* visualization method and compared the results, which indicated a suitable accuracy.

Finally, several approaches to CFD investigation for the characterization of RPBs, published in 2010–2020, are summarized in Table 6. According to this table, it is clear that the obstacle, *VOF* and realizable models were more attractive to, and more widely applied by, researchers.

Table 6. Models recently applied by various investigators for CFD analysis.

Physical Model	Dimensions	Multiphase Model	Turbulence Model	Solving Approach	Scope	Published Year	Refs.
Obstacle	2D and 3D	Single phase	Realizable k-ε	—	Pressure field and gas flow characteristics analysis	2010	[176]
Porous	3D	—	Standard k-ε	—	Pressure field and hydrodynamic analysis	2012	[177]
Obstacle	2D	Single phase	Standard k-ε	SIMPLE	Hydrodynamic analysis	2013	[184]
Obstacle	2D	*VOF*	RSM	SIMPLE	Hydrodynamic analysis	2013	[178]
Porous	3D	Euler	Standard k-ε	—	Hydrodynamic analysis	2013	[185]
Obstacle	2D	DPM	RNG k-ε	SIMPLE	Mixing and droplet size analysis	2014	[179]
Obstacle	3D	*VOF*	RNG k-ε	PISO/ PRESTO	Hydrodynamic and MT analysis	2014	[180]
Obstacle	2D	*VOF*	RSM	SIMPLE	Micro-mixing efficiency analysis	2016	[186]
Obstacle	2D	*VOF*	—	PISO/ PRESTO	Hydrodynamic and MT analysis	2017	[187]
Real	3D	Single phase	Realizable k-ε	—	Pressure drop and gas flow characteristics analysis	2017	[183]
Obstacle	2D	*VOF*	*SST* k-ω	PISO/ PRESTO	Hydrodynamic analysis	2017	[188]
Obstacle	2D & 3D	*VOF*	Realizable k-ε, RSM, k-ω	SIMPLE	Hydrodynamic and droplet size analysis	2017	[189]
Obstacle	2D	*VOF*	Realizable k-ε	SIMPLE/PRESTO	Micro-mixing efficiency analysis	2018	[190]
Porous	2D and 3D	Single phase	Realizable k-ε	SIMPLE	Gas flow characteristics analysis	2018	[191]
Obstacle	2D	*VOF*	Standard k-ε	SIMPLE	Hydrodynamic analysis	2018	[192]
Obstacle	3D	Single phase	Standard k-ε	SIMPLE/PRESTO	Droplet behaviors	2019	[193]
Obstacle	2D	*VOF*	Realizable k-ε	PISO	Hydrodynamic analysis	2019	[194]
Obstacle	2D	*VOF*	Realizable k-ε	SIMPLE/PRESTO	Micro-mixing efficiency analysis	2019	[195]
Obstacle	2D	*VOF*	Realizable k-ε	SIMPLE/PRESTO	Hydrodynamic analysis	2019	[66]
Obstacle	2D	*VOF*	RSM	PISO/ PRESTO	MT analysis	2016	[181]
Real	2D	*VOF*, Euler	RSM, *LES*	—	Hydrodynamic and liquid behavior analysis	2019	[196]
REU	3D	*VOF*	*SST* k-ω	PISO	Hydrodynamic analysis	2019	[170]
Obstacle	3D	*VOF*	*SST* k-ω	SIMPLE	Hydrodynamic and liquid behavior analysis	2019	[197]
Real	3D	Single phase	Realizable k-ε	SIMPLE C/PRESTO	Gas flow characteristics analysis	2020	[198]

DPM: Lagrange discrete phase mode.

4. Dimensional Analysis

There are several approaches to scaling up in addition to dimensional analysis (DA). For instance, G. Jan Harmsen [199] divided the scale-up process in a pilot plant into the following categories, and recommended the following classifications for PI:

1. Brute force;
2. Rate model.

The DA method was used in this section due to the lack of data on scale-up methods for RPBs analysis. Several important parameters are required for the scaling up of RPBs, such as MT parameters, hydrodynamic information, etc., which can be found via several means, such as fundamental investigations or CFD analysis, as discussed in previous sections. DA can help to create more accurate and unique design parameters. In agitation contactors, the power requirement per unit volume and the mixing quality or fluid behavior are the scale-up criteria [200,201]. The same is true of an RPB, but the geometry and configuration of the rotor are different here; therefore, it is clear that the high-gravity factor should be a dimensionless number that may be used in gravity field analysis (as defined by Equation (53)), as employed by Jiao et al. [130] to study the gas pressure drop and MT in CO_2–NaOH system. This study demonstrated that this parameter linearly increased with the radii of the rotor at a constant rate.

$$\lambda = \frac{\omega^2 r}{g} \tag{53}$$

Youzhi Liu et al. [69] examined the effects of this dimensionless parameter in a special RPB and an *RSB*, and showed that $K_G a$, a and k_y were augmented when λ increased. This dimensionless number enhanced the contacting situation, with finer droplets and increased MT when its value was increased, as Gui and Li [202] pointed out. S. B. Cao et al. [161] reported that a high λ value caused a change in the liquid flow pattern in the packing, from liquid film to droplets and small filaments, as follows:

1. liquid films $\lambda < 60$ g;
2. liquid droplets and small filaments $\lambda > 100$ g.

Additionally, their experimental results indicate that an increase in λ could reduce the *HTU* and increase $K_G a$ significantly.

It is worth noting that a correlation that considers *Re*, *Sc* and *Sh* only could not be suitable for MT coefficient prediction, because packing geometry is not included [203]. In light of this, Rajan et al. [121] reported that the Reynolds, Froude, and Weber numbers are the other important dimensionless numbers for determining the functions of $u_{L,s}$, and they could change with the radios of the RPB and u_g. Furthermore, a_c and a_t can affect the Froude and Weber numbers, respectively. Xu et al. [179] reported hydrodynamic similarity as another criterion required for effective scaling up. The Weber number reflects the droplets' break-up status inside the packing, and is defined as the ratio of the inertial force to the surface tension; its value increases as the rotor speed increases. Moreover, B. Zhao et al. [75] developed a model that uses dimension analysis, and defined three issues that could influence the RPB's performance, namely, gas–liquid properties, operation conditions, and geometrical dimensions.

In light of all of the above, we have clarified the parameters that could affect performance—applying the Buckingham π theory to do so—and outlined the five independent dimensionless numbers of Re_G, Re_L, Sc_G, Sc_L, *Mr*, and *Sh* as dependent dimensionless numbers. Hence, the following correlation was proposed:

$$Sh = 3.788 \times 10^{-6} Re_G^{0.1404} Re_L^{0.3684} Sc_L^{1.2280} Gr_G^{0.0337} Mr^{0.4286} \tag{54}$$

where *Sh* indicates the effective convective MT, and the exponent values of the *Gr* and *Re* numbers indicate the degree of turbulence [204].

Regarding the geometrical dimensions, it must be noted that the geometry of an RPB can influence the *Re*, *Gr* and *Sc* via changes in the average radial gas velocity and MT coefficients [205].

The Hatta number (*Ha*) is another important dimensionless number in RPBs incorporating a reaction system. This number is useful in comparing the reaction rate in the liquid film with the diffusion rate. For instance, S. Munjal et al. described this number for CO_2 absorption with NaOH solution, using a pseudo first-order reaction. The value of this dimensionless number exceeds 1 for fast reaction rates, while a value of lower than 1 indicates that physical absorption overcomes the kinetic reaction.

Gas treatment capacity, τ, is another variable to consider when characterizing the parameters of RPBs, as highlighted by Sheng et al. [172]. This factor can be used to scale up and determine the processing capacity, which is described by Equation (55).

$$\tau = \frac{Q_G}{V_b \times 10^6} \tag{55}$$

Additionally, as Neumann et al. [4,114] showed in 2017 and 2018, two considerable factors, maximum and integrated gas capacity and maximum and integrated liquid load, could be applied for benchmarking RPBs.

5. Power Consumption

Keyvani and Gardner [206] reported that the total power consumption of RPBs, as shown in Figure 6, includes rotor power consumption, mechanical friction, and friction loss due to liquid passing through the bed. Singh et al. [119] defined this parameter as follows:

$$N_t = 1.2 + 1.1 \times 10^{-3}\left(\rho_L R_o^2 \omega^2 Q_L\right) \tag{56}$$

and for *CRB*s, Wang et al. [128] proposed the following correlation:

$$N_{tot} = 5.5n^{0.67} + 0.338nQ_{s,L}^{0.16}u_g^{0.33} \tag{57}$$

Agarwal et al. developed a model to calculate the total power consumption of *RSB*s via Equation (58) [207]:

$$N_{tot} = 1.2 + 1.1 \times 10^{-3}\rho_L Q_L r_o^2 \omega^2 + \frac{\rho_L \omega Q_L^2 \{2r_i(s+1/2) + s(s+1)(w+t)\}}{4\pi hl} \times 10^{-3} \tag{58}$$

As Jiang et al. reported, high rotational speeds in RPBs cause increases in the device cost [208].

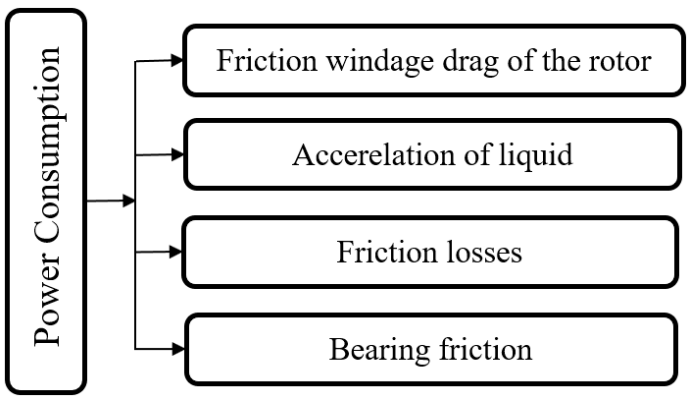

Figure 6. Total power consumption in different sections of RPBs.

Jonathan Lee et al. [209] calculated the total power consumption of a simple counter-current RPB equipped with a stainless steel mesh, using Equation (59):

$$N_{tot} = \omega_m L_{tor} F_{tor} \quad (59)$$

where ω_m is the rotational speed of the motor (1/s), L_{tor} is the torque arm length (m), and F_{tor} is the force required to hold the torque arm horizontal (N).

Finally, it is worth noting that detailed cost estimation formula have been developed for RPBs by Gudena et al. [122].

6. Future Perspective

Analyses and evaluations of the above research results show that further research is required for achieving MT and reaction models with greater result transparency; wet and effective interfacial gas–liquid surface area measurements, computed with theoretical and empirical models for physical absorption and volumes in the cavity, bulk, and end-effect zones in various kinds of RPB with different kinds of packing; the analysis of MT rate computations and liquid distribution patterns in *RSB*s and *RZB*s. It is also clear that conceptual systematic dimensional analysis, rigorous scale-up methods, cost estimation, residence time, and power consumption formulations with greater accuracy require further study as well. Other subjects that can be considered in future investigations include the effects of magnetic fields (DC and AC) and ultrasonic induction on the MT and hydrodynamics in RPBs when ionic fluids or nanofluids are employed as the solvent; the development of more suitable and accurate models for the simplification of various kinds of packing, hydrodynamics and mass transfer analyses for wire mesh packing, especially when the layers of mesh are placed together horizontally, as in a sandwich, rather than vertically, as in [149]; performance comparisons between RPBs and PBCs in terms of the MT rate and the reduction in energy consumption in the stripping process when using nanofluids or other advanced solvents; the analysis of industrial applications, which can reduce the environmental effects, especially with the use of CFD tools; finally, more 3D CFD simulations of multiphase RPBs to investigate the real definition of hydrodynamics and MT, and the further development of simple and acceptable accuracy models to define porous media that can reduce the time and cost of computation, especially in 3D simulations.

7. Conclusions

In this study, a comprehensive review was conducted of the process intensification equipment used for gas absorption processes, which are known as rotating packed beds (RPB) or HiGee contactors. Using centrifugal acceleration in RPBs intensifies the MT coefficient, and this leads to a reduction in the packing volume and energy consumption in comparison with packed beds. The gas velocity and flow area change radially in RPBs; therefore, MT coefficients change from point to point in contactors, but there is no general theory for this, and the prediction of MT coefficients in RPBs is theoretically complicated. Past investigations have shown that the local $K_G a$ in the end-effect zone is higher than the value of this coefficient in the bulk zone of the packing, and the MT coefficient strongly depends on the hydrodynamics of two phases. Therefore, further evaluation of this subject is necessary to improve and optimize RPBs. Previous studies have shown that MT coefficients are increase by reductions in boundary layer thickness, as a result of which the *HTU* will be decreased. Then, the liquid hold-up and pressure drop in RPBs were investigated. Past researchers have demonstrated that suitable dimensionless numbers, such as *Re*, *Ga*, and *Ka*, make hold-up predictions more accurate. Research results have shown that pressure drops are mainly related to the outer radius of the RPB and its packing type. Moreover, a suitable estimation of pressure drop can be achieved using the channel model. Moreover, by adding blades and baffles, one can reduce the total pressure. Unlike in PBCs, the effective MT surface area is not equal to the wet surface area or total surface area in RPBs. A contact area covered by flying droplets, which can be defined by the *We* number, affects the size of the effective surface area in RPBs. Previous studies have demonstrated

that, in addition to the packing type, a good distribution of the fluid increases the effective surface area in the cavity and packing zones, and is considered as a parameter that effects flooding. The dimensionless numbers that affect MT description correlations are *Re*, *Gr*, *Sc*, *Fr* and *We*, which were recently improved by adding the geometry factor. The MT rate can be changed locally via the alteration of the flow area, gas, and liquid velocity. CFD and dimensional analysis are efficient tools for studying the RPB. CFD is a suitable tool for surveying hydrodynamic details and the MT rate. The results reveal that, for the achievement of maximum accuracy in the modeling of RPB in the gas–liquid transition process, one can use innovative models that use CT reconstruction for the generation of packing geometry, the *VOF* model for two-phase modeling, and the realizable k-ε turbulence model for hydrodynamic analysis. Dimensional analysis is an efficient method for the scaling up and benchmarking of RPB systems.

Author Contributions: The present research has been prepared and compiled by all three authors. The main idea of this investigation was performed by all three authors. The literature review was conducted by F.G. under the supervision of A.A. in consultation with A.V. The main structure of this review paper was done in consultation with all three authors. This review paper was written and reviewed by F.G., reviewed and analyzed by A.A. and supervised by A.V. The management of compiling and analyzing the results of this research was done by A.A. The manuscript of this review paper has been approved by all three authors. All authors have read and agreed to the published version of the manuscript.

Funding: This research received no external funding.

Institutional Review Board Statement: Not applicable.

Informed Consent Statement: Not applicable.

Data Availability Statement: Not applicable.

Conflicts of Interest: The authors declare no conflict of interest.

Nomenclature

a	Effective gas–liquid surface (interfacial) area per unit volume of the packed bed, m^2/m^3
a_c	Centrifugal acceleration, $= \omega^2 r_{avg}$ m/s^2
a_e,a_s	Specific surface area, m^2/m^3
a_t	Surface area of the packing per unit volume of the bed, m^2/m^3
a_w	Wetted surface area, m^2/m^3
A, B, C	Experimental constant,
$C_{i,\,CO_2}$	Absorbing component (CO_2) inlet concentration, ppm
$C_{o,\,CO_2}$	Absorbing component (CO_2) outlet concentration, ppm
C_a	Concentration of absorbent media, mol/L or g/L
C_s	Concentration of absorbent salt, g/L
$C_{CO_2}{}^*$	$C^*_{CO_2} = H_{CO_2} P_{CO_2}$
d	Diameter of packing or equivalent spherical diameter $= \frac{6(1-\varepsilon)}{a_t}$, m
d_b	Average droplet diameter in bulk zone, m
d_e	Average droplet diameter in end zone, m
d_h	Hydraulic diameter, m
d_i	Inner diameter of *RZB* rotor, m
d_o	Inner diameter of *RZB* rotor, m
d_p	Pore diameter, mm
d_N	Diameter of nozzles, mm
d_w	Dimeter of wire/fiber, mm
$\overline{d}$	Average diameter of droplet, mm
d_1	Diameter of droplet at demarcation point, m
D	Diffusivity of the phase, m^2/s

D_i	Inner diameter of the casing of rotating bed, m
E	Reaction enhancement factor
E_i	Instantaneous reaction enhancement factor
f	Friction factor in RPB or friction coefficient of mechanical seal in *RZB*s
f_d	The fraction of volume the liquid distributer occupies in the inner radius of RPBs
f_G	Dry resistance coefficient, which depends on the Q_G and ω
f_w	Wetted resistance coefficient, which depends on Q_L, ω and β,
$\overline{F}_{G,int} : \overline{F}_{L,int} : F_v$	*F*-factor, $kg^{1/2}/m^{1/2}s$
g	Gravitational acceleration of earth, m/s^2
G	Gas mass flow rate, kg/s or kg/h
h	The (axial) height of packing in RPBs or the height of the annual space at the inner edge of the *RZB*'s rotor, m
h_c	The height of the concentric rings, rotors and packing beds in *CRB*s, m
h_f	The minimum height of the RPB required to prevent its operation in a flooding regime
H	Henry's constant, $atm.m^3/mol$
H_s	Solubility coefficient of CO_2 in solution, $kmol/m^3 \cdot Pa$
HTU	Height of a transfer unit, m
k_G	Gas phase mass transfer coefficient, $g\ mol/(atm \cdot m^2 \cdot s)$
k_L	Liquid phase mass transfer coefficient, m/s
k_1	Reaction rate constant, m^3/s
k_2	Second-order rate of reaction, $m^3/kmol \cdot s$
$k_2^{\infty} K$	Collision kinetic energy loss
$K_G a$	Overall volumetric gas phase mass transfer coefficient, $gmol/(atm \cdot m^3 \cdot s)$
$K_L a$	Overall volumetric liquid phase mass transfer coefficient, 1/s
K_1	Departure coefficient of gas (the departure of power for a real liquid flow with a gas flow equal to zero) in *RZB*s
K_2	Departure coefficient of real liquid (the departure of power for a real liquid flow from that of the ideal liquid flow when no gas flows through the rotor) in *RZB*s
k_R	Pseudo first-order rate constant, 1/s
L, $\dot{L}$	Liquid mass flow rate, kg/s or kg/h
L_p	Perimeter of rotational baffle channel in contact with fluid, m
$\dot{m}$	Mass flow rate, kg/s or ton/h
n or N	Rotational speed, rpm and number
N_G	Power requirement for a gas flow through the rotor, W
N_i	Absorption rate of a component, $kmol/m^2 \cdot s$
N_L	Power requirement for the liquid flow through the rotor, including liquid acceleration and friction losses, W
N_{LD}	Power transmitted to liquid flow by a rotation disk and rotational baffles for the ideal liquid flow at a zero gas flow, W
N_{LR}	Power requirement for a liquid flow at a zero gas flow, W
N_M	Power requiremnt due to mechanical friction, proportional to ω, W
N_w	Power requiremnt due to frictional windage drag of a rotor, proportional to $\omega^{1.5}$, W
N_{tot}	Total power (Load) consumption, W
N_T	Number of theoretical trays
P_c	Pressing pressure between the stationary and rotational rings in *RZB*s
ΔP	Total pressure drop, kPa
ΔP_c	Pressure drop due to centrifugal force, kPa
ΔP_{cw}	Wet pressure drop due to centrifugal force without a gas flow, kPa
ΔP_d	Dry pressure drop, kPa
ΔP_f	Pressure drop due to frictional force, kPa
ΔP_k	Pressure drop due to kinetic energy, kPa
ΔP_m	Pressure drop due to momentum gain by gas radial motion in rotors, kPa
ΔP_w	Wet pressure drop, kPa
ΔP_{Ts}	Total pressure drop through stationary rotors (of *RSB*s), kPa
q	Dimensionless initial velocity of liquid
Q	Flow rate, m^3/h
$Q_{C,\,CO_2}$	Captured CO_2, L/min

Q_{CO_2}	CO_2 flow rate, L/min
Q_m	Minimum wetting rate of packing, $m^3/m{\cdot}h$
Q_s	Specific flow rate, m^3/h
r	Radius of packing or coordinate direction parallel to disk surface, m
r_{avg}	Average radius of a packed bed, m
r_{RB}	Radius of rotational baffle in *RZB*s, m
r_i	Inside radial length of packing, mm
r_o	Outside radial length of packing, mm
r_h	Hydraulic radius, m
r_s	Radius of the stationary housing, m
r_{M1}	Outer radius of the annular face with a stationary ring against the rotating ring in *RZB*s, m
r_{M2}	Inner radius of the annular face with a stationary ring against the rotating ring in *RZB*s, m
Δr	Distance between the rotational and stationary baffles, m
R_{CO_2}	Rate of CO_2 absorption per unit volume, $mol/m^3{\cdot}s$
R_i	Inner rotor radius, m
R_o	Outer rotor diameter, m
R_p	Quadratic mean of radius of packing, m
s	Number of packing splits in *RSB*
S	Area of rotational baffle channel through which fluid passes in a radial direction, m^2
t	Treatment time, min
$\bar{t}$:T	Temperature, K
$\overline{u_L}$	Liquid mean radial velocity, m/s
$u_{L,r}$	Liquid velocity in the radial direction, m/s
u_g	Gas superficial velocity, m/s
$u_{L,s}$	Liquid superficial velocity, m/s
u_{jet}	Liquid jet velocity, m/s
u_0	Liquid initial velocity, m/s
u_θ	Gas tangential velocity, m/s
V_b	Packing volume = $\pi(r_o^2 - r_i^2)h$, m^3
V_i	Volume inside the inner radius of the bed, m^3
V_o	Volume between the outer radius of the bed and the stationary housing, m^3
V_L	The volume held by liquid in the packing, m^3
W_{TEG}	*TEG* concentration, %
Y	Mole fraction, %
Y_i	Mole fraction of a component in the inlet gas stream, %
Y_o	Mole fraction of a component in the outlet gas stream, %
Y_w	Mole fractions of water in a gas phase, %
Y^*	Gas phase mole fraction of CO_2 in equilibrium with the concentration of CO_2 in liquid

Abbreviations

AMP	2-amino-2-mthyl-1-propanol
ATU	area per transfer unit, m^2
CCD	Charge-coupled device camera
CRB	Concentric ring rotating bed
DEA	Diethanolamine
DEAB	4-diethylamino-2-butanol
DEEA	*N*,*N*-diethyl ethanolamine
DIPA	Diisopropandamine
DMEA	*N*,*N*-dimethyl ethanolamine
1DMA2P	1-dimethylamino-2-propanol
DO	Dissolved oxygen in water
GS	Gamma scanning
LDV	Laser doppler velocimetry
LIF	Laser-induced fluorescence

LES	Large eddy simulation
IPA	Isopropyl alcohol
HETP	Height equivalent to a theoretical plate
MEA	Monoethanolamine
MDEA	Methyldiethanolamine
NMP	*N*-methyl-2-pyrrolidone
NTU	number of transfer units
PIV	Particle image velocimetry
PZ	Piperazine
RSB	Rotating split bed
RTNR	Real-time neutron radiography
RZB	Rotating zigzag bed
SST	Shear–stress transport
TEG	Triethylene glycol
VOF	Volume of fluid
XCT	X-ray computational tomography scanner

Greek Letters

β	Liquid hold-up, volume of liquid sustained per unit volume of packing, dimensionless
β_v	mean saturation of packing, the ratio of the overall liquid volume and of the PB total void volume
$<\beta>$	radial saturation mean of the RPB
γ	Contacting angle, degree
δ	Liquid film thickness, m
$\overline{\delta}$	Mean thickness of liquid, m
ε	Porosity of packing
ζ	Liquid maldistribution of injector, %
ν	Kinematic viscosity of liquid, m^2/s
ρ	density, kg/m^3
ω	Angular speed, rad/s or s^{-1}
σ	Surface tension of liquid, N/m or kg/s^2
σ_w	Surface tension of water in 25 °C, 0.072 kg/s^2
σ_c	Critical surface tension of packing, N/m or kg/s^2
ξ	the ratio of liquid jet to the exit-gas kinetic energy
φ	Fractional opening area of rotational baffle in *RZB*s, dimensionless shape factor number
λ	Gravity factor
τ	Gas treatment capacity of packing, 1/hr

Subscripts

B, *b*	Packing
L	Liquid phase
G	Gas phase
W	Water
IMZ	Inner wire mesh packing zone
OPZ	Outer resin pin zone

Dimensionless groups

A	Absorption factor, $= \frac{Q_L}{HQ_G}$
Ca	Capillary number
Froude number	$Fr = \frac{Q_L^2 a_t}{\rho_L^2 g}$
Galileo number	$Ga = \frac{g d_p^3 \rho_L^2}{\mu_L^2}$
Hatta numbers	$Ha = \frac{\sqrt{k D_{CO_2} C_{OH^-}}}{k_L}$ (where k is reaction rate constant of CO_2, $m^3/kmol{\cdot}s$ in case of NaOH solution)

H_y	Dimensionless Henry's constant
Kapitza number	$Ka = \frac{\mu^4 r\omega^2}{\rho\sigma^3}$
Modified Galileo number	$Ga^* = \frac{d^3\rho_L\left(\rho_L a_c - \frac{\Delta P}{r_o - r_i}\right)}{\mu_L^2}$
Molar Ratio	$Mr = \frac{Q_L C_a}{Q_G C_i}$
Ohnesorge number	$Oh_{in} = \frac{\mu_L}{\sqrt{\rho_L \sigma d_m}}$
Reynolds number	$Re = \frac{ud_p}{(2\pi Rh)\nu_L}$
	$Re_{in} = \frac{\rho_L u_r d_m}{\mu_L}$
Particle Reynolds number	$Re_p = \frac{\dot{m}_g d_p}{\mu_g}$
Rotational Reynolds number	$Re_\omega = \frac{\omega r_{avg}^2}{\nu_L}$
Schmidt number	$Sc = \frac{\mu}{\rho D}$
Weber number	$We = \frac{Q_L^2 \rho_L d_p}{(2\pi Rh)^2 \sigma}$

References

1. Reay, D. The Role of Process Intensification in Cutting Greenhouse Gas Emissions. *Appl. Therm. Eng.* **2008**, *28*, 2011–2019. [CrossRef]
2. Harmsen, J. Process Intensification in the Petrochemicals Industry: Drivers and Hurdles for Commercial Implementation. *Chem. Eng. Process. Process Intensif.* **2010**, *49*, 70–73. [CrossRef]
3. Keil, F.J. Process Intensification. *Rev. Chem. Eng.* **2018**, *34*, 135–200. [CrossRef]
4. Neumann, K.; Gladyszewski, K.; Groß, K.; Qammar, H.; Wenzel, D.; Górak, A.; Skiborowski, M. A Guide on the Industrial Application of Rotating Packed Beds. *Chem. Eng. Res. Design.* **2018**, *134*, 443–462. [CrossRef]
5. Stankiewicz, A.I.; Moulijn, J.A. Process Intensification: Transforming Chemical Engineering. *Chem. Eng. Prog.* **2000**, *96*, 22–34.
6. Rao, D.P. The Story of "HIGEE". *Indian Chem. Eng.* **2015**, *57*, 282–299. [CrossRef]
7. Ehinmowo, A.; Aliyu, A.; Alagbe, S.; Adedipe, O.; Olumi, O. Offshore Topside Rotating Packed Bed as Process Intensified Alternative for Natural Gas Sweetening and Dehydration. *Am. Chem. Sci. J.* **2015**, *8*, 1–12. [CrossRef]
8. Ramshaw, C.; Mallinson, R.H. Mass Transfer Process. U.S. Patent 4,283,255A, 11 August 1981.
9. Peel, J.; Howarth, C.R.; Ramshaw, C. Process Intensification: Higee Seawater Deaeration. *Chem. Eng. Res. Des.* **1998**, *76*, 585–593. [CrossRef]
10. Garcia, G.E.C.; Van Der Schaaf, J.; Kiss, A.A. A Review on Process Intensification in HiGee Distillation. *J. Chem. Technol. Biotechnol.* **2017**, *92*, 1136–1156. [CrossRef]
11. Guo, J.; Jiao, W.; Qi, G.; Yuan, Z.; Liu, Y. Applications of High-Gravity Technologies in Gas Purifications: A Review. *Chin. J. Chem. Eng.* **2019**, *27*, 1361–1373. [CrossRef]
12. Merkel, T.C.; Lin, H.; Wei, X.; Baker, R. Power Plant Post-Combustion Carbon Dioxide Capture: An Opportunity for Membranes. *J. Memb. Sci.* **2010**, *359*, 126–139. [CrossRef]
13. Kunze, C.; Spliethoff, H. Assessment of Oxy-Fuel, Pre- and Post-Combustion-Based Carbon Capture for Future IGCC Plants. *Appl. Energy* **2012**, *94*, 109–116. [CrossRef]
14. Kang, J.L.; Wong, D.S.H.; Jang, S.S.; Tan, C.S. A Comparison between Packed Beds and Rotating Packed Beds for CO_2 Capture Using Monoethanolamine and Dilute Aqueous Ammonia Solutions. *Int. J. Greenh. Gas Control* **2016**, *46*, 228–239. [CrossRef]
15. Yeh, J.T.; Pennline, H.W.; Resnik, K.P. Study of CO_2 Absorption and Desorption in a Packed Column. *Energy Fuels* **2001**, *15*, 274–278. [CrossRef]
16. Pourkargar, D.B.; Shahri, S.M.K.; Rioux, R.M.; Armaou, A. Spatiotemporal Modeling and Parametric Estimation of Isothermal CO_2 Adsorption Columns. *Ind. Eng. Chem. Res.* **2016**, *55*, 6443–6453. [CrossRef]
17. Rosli, S.S.; Wong, C.Y.; Yunus, N.M.; Lam, M.K.; Show, P.L.; Cheng, C.K.; Wang, D.K.; Da Oh, W.; Lim, J.W. Optimum Interaction of Light Intensity and CO_2 Concentration in Bioremediating N-Rich Real Wastewater via Assimilation into Attached Microalgal Biomass as the Feedstock for Biodiesel Production. *Process Saf. Environ. Prot.* **2020**, *141*, 355–365. [CrossRef]
18. Harbold, G.; Park, J. Using the GasTran Deaeration System to Achieve Low Dissolved Oxygen Levels for Superior Line Speed and Product Quality: A Case Study in Carbonated Soft Drink Bottling. In Proceedings of the 7th International Conference on Process Intensification, Albany, NY, USA, 15–17 September 2008.
19. Hosseinzadeh, A.; Hosseinzadeh, M.; Vatani, A.; Mohammadi, T. Mathematical Modeling for the Simultaneous Absorption of CO_2 and SO_2 Using *MEA* in Hollow Fiber Membrane Contactors. *Chem. Eng. Process. Process Intensif.* **2017**, *111*, 35–45. [CrossRef]
20. Thiels, M.; Wong, D.S.; Yu, C.-H.; Kang, J.-L.; Jang, S.S.; Tan, C.-S. Modelling and Design of Carbon Dioxide Absorption in Rotating Packed Bed and Packed Column. *IFAC-PapersOnLine* **2016**, *49*, 895–900. [CrossRef]
21. Cheng, H.-H.; Lai, C.-C.; Tan, C.-S. Thermal regeneration of alkanolamine solutions in a rotating packed bed. *Int. J. Greenh. Gas Control.* **2013**, *16*, 206–216. [CrossRef]

22. Mohammaddoost, H.; Azari, A.; Ansarpour, M.; Osfouri, S. Experimental investigation of CO_2 removal from N2 by metal oxide nanofluids in a hollow fiber membrane contactor. *Int. J. Greenh. Gas Control.* **2018**, *69*, 60–71. [CrossRef]
23. Luo, Y.; Luo, J.-Z.; Yue, X.-J.; Song, Y.-J.; Chu, G.-W.; Liu, Y.; Le, Y.; Chen, J.-F. Feasibility studies of micromixing and mass-transfer in an ultrasonic assisted rotating packed bed reactor. *Chem. Eng. J.* **2018**, *331*, 510–516. [CrossRef]
24. Song, C.; Liu, Q.; Ji, N.; Deng, S.; Zhao, J.; Li, Y.; Song, Y.; Li, H. Alternative pathways for efficient CO_2 capture by hybrid processes—A review. *Renew. Sustain. Energy Rev.* **2018**, *82*, 215–231. [CrossRef]
25. Sang, L.; Luo, Y.; Chu, G.-W.; Liu, Y.-Z.; Liu, X.-Z.; Chen, J.-F. Modeling and experimental studies of mass transfer in the cavity zone of a rotating packed bed. *Chem. Eng. Sci.* **2017**, *170*, 355–364. [CrossRef]
26. Yue, X.-J.; Luo, Y.; Chen, Q.-Y.; Chu, G.-W.; Luo, J.-Z.; Zhang, L.-L.; Chen, J.-F. Investigation of micromixing and precipitation process in a rotating packed bed reactor with PTFE packing. *Chem. Eng. Process. Process. Intensif.* **2018**, *125*, 227–233. [CrossRef]
27. Guo, F.; Zheng, C.; Guo, K.; Feng, Y.; Gardner, N.C. Hydrodynamics and mass transfer in cross-flow rotating packed bed. *Chem. Eng. Sci.* **1997**, *52*, 3853–3859. [CrossRef]
28. Liu, H.-S.; Lin, C.-C.; Wu, S.-C.; Hsu, H.-W. Characteristics of a Rotating Packed Bed. *Ind. Eng. Chem. Res.* **1996**, *35*, 3590–3596. [CrossRef]
29. Tsai, C.-Y.; Chen, Y.-S. Effective interfacial area and liquid-side mass transfer coefficients in a rotating bed equipped with baffles. *Sep. Purif. Technol.* **2015**, *144*, 139–145. [CrossRef]
30. Munjal, S.; Dudukovć, M.P.; Ramachandran, P. Mass-transfer in rotating packed beds—I. Development of gas—liquid and liquid—solid mass-transfer correlations. *Chem. Eng. Sci.* **1989**, *44*, 2245–2256. [CrossRef]
31. Munjal, S.; Dudukovi ć, M.P.; Ramachandran, P. Mass-transfer in rotating packed beds—II. Experimental results and comparison with theory and gravity flow. *Chem. Eng. Sci.* **1989**, *44*, 2257–2268. [CrossRef]
32. Lin, C.C.; Chien, K.S. Mass-Transfer Performance of Rotating Packed Beds Equipped with Blade Packings in VOCs Absorption into Water. *Sep. Purif. Technol.* **2008**, *63*, 138–144. [CrossRef]
33. Chen, Y.H.; Chang, C.Y.; Su, W.L.; Chen, C.C.; Chiu, C.Y.; Yu, Y.H.; Chiang, P.C.; Chiang, S.I.M. Modeling Ozone Contacting Process in a Rotating Packed Bed. *Ind. Eng. Chem. Res.* **2004**, *43*, 228–236. [CrossRef]
34. Jassim, M.S.; Rochelle, G.; Eimer, D.; Ramshaw, C. Carbon Dioxide Absorption and Desorption in Aqueous Monoethanolamine Solutions in a Rotating Packed Bed. *Ind. Eng. Chem. Res.* **2007**, *46*, 2823–2833. [CrossRef]
35. Zheng, C.; Guo, K.; Feng, Y.; Yang, C.; Gardner, N.C. Pressure Drop of Centripetal Gas Flow through Rotating Beds. *Ind. Eng. Chem. Res.* **2000**, *39*, 829–834. [CrossRef]
36. Sandilya, P.; Rao, D.P.; Sharma, A.; Biswas, G. Gas-Phase Mass Transfer in a Centrifugal Contactor. *Ind. Eng. Chem. Res.* **2001**, *40*, 384–392. [CrossRef]
37. Cheng, H.H.; Tan, C.S. Carbon Dioxide Capture by Blended Alkanolamines in Rotating Packed Bed. *Energy Procedia* **2009**, *1*, 925–932. [CrossRef]
38. Lin, C.C.; Lin, Y.H.; Tan, C.S. Evaluation of Alkanolamine Solutions for Carbon Dioxide Removal in Cross-Flow Rotating Packed Beds. *J. Hazard. Mater.* **2010**, *175*, 344–351. [CrossRef]
39. Chu, G.W.; Luo, Y.; Shan, C.Y.; Zou, H.K.; Xiang, Y.; Shao, L.; Chen, J.F. Absorption of SO_2 with Ammonia-Based Solution in a Cocurrent Rotating Packed Bed. *Ind. Eng. Chem. Res.* **2014**, *53*, 15731–15737. [CrossRef]
40. Lin, C.-C.; Chen, B.-C. Carbon Dioxide Absorption into NaOH Solution in a Cross-Flow Rotating Packed Bed. *J. Ind. Eng. Chem.* **2007**, *13*, 1083–1090.
41. Podbielniak, W.J. Centrifugal Fluid-Treating Apparatus and Seal. Google Pat. 2172222, 5 September 1939.
42. Podbielniak, W.J. Art of Effecting Countercurrent Contact between Fluids. U.S. Patent 2,281,796, 8 March 1935.
43. Podbielniak, W.J. Centrifugal Countercurrent Exchange Device. U.S. Patent 2758783A, 5 November 1951.
44. Podbielniak, W.J. Centrifugal Countercurrent Contacting Method and Apparatus. U.S. Patent 2878993, 5 July 1959.
45. Wilhelm, P.C.; Wilhelm, D.S. Apparatus for Intimate Contacting of Two Fluid Media Having Different Specific Weight. U.S. Patent 2,941,872, 9 June 1960.
46. Pilo, C.W.; Dahlbeck, S.W. Means for the Distribution of a Liquid on Rotating Surfaces. U.S. Patent 3034730, 23 September 1962.
47. Podbielniak, W.J. Continuous Centrifugal Vaporliquid Contactor. U.S. Patent 3,233,880, 3 August 1962.
48. Podbielniak, W.J. Centrifugal Apparatus with Axially-Extended Rotor. U.S. Patent 3,344,981, 8 February 1965.
49. Pilo, C.W. Centrifugal Contact Apparatus. U.S. Patent 3,415,501, 27 December 1965.
50. Todd, D.B. Multistage Vapor-Liquid Contactor. U.S. Patent 3,486,743, 16 June 1967.
51. Pilo, C.W. Rotary Gas Washers. U.S. Patent 4,397,794, 7 December 1981.
52. Yang, S.; Lin, C.-C.; Tseng, I.-M.; Liu, W.-T.; Yu, H.-T. Method for Removing Volatile Components from a High Viscosity Liquid by Using Rotation Pack Bed. U.S. Patent 6,884,401 B2, 17 July 2002.
53. Ji, Z.J.; Xu, Y.Y. Equipment of Zigzag High-Gravity Rotating Beds. U.S. Patent 7,344,126 B2, 12 April 2004.
54. Marcus, D.E.M.; Mannel, L.; Krishniah, P.; David, B. Liquid Distributor for a Rotating Packed Bed. U.S. Patent 8,448,926 B2, 9 June 2011.
55. Hartwing, W.; Petar, A.; Klaus Ennebach, M.H.T. Rotating Packed Bed. U.S. Patent 20130319235A1, 3 August 2012.
56. Murali, K.; Namdeo, B.K.; Gandham, S.G.; Sheshachala, S.N.; Annaji, R.K.T. Rotating Packed Bed Unit. U.S. Patent 2016/0317967 A1, 16 November 2016.

57. Namdeo, B.K.; Gandham, G.; Sheshachala, S.N.; Annaji, R.K.T. Rotating Packed Bed Assembly. U.S. Patent 20170028311A1, 2 February 2017.
58. Tan, C.H.; Yu, C.S. Apparatus for Absorbing a Component from a Gas Mixture. U.S. Patent 20170157554A1, 8 June 2017.
59. E Mello, M.V.D.; Huang, H.-M. System and Methods for Deaerating Sea Water Using a Rotating Packed Bed. U.S. Patent 20180016159A1, 18 January 2018.
60. Lin, C.C.; Chu, C.R. Feasibility of Carbon Dioxide Absorption by NaOH Solution in a Rotating Packed Bed with Blade Packings. *Int. J. Greenh. Gas Control* **2015**, *42*, 117–123. [CrossRef]
61. Liu, Y.; Gu, D.; Xu, C.; Qi, G.; Jiao, W. Mass Transfer Characteristics in a Rotating Packed Bed with Split Packing. *Chin. J. Chem. Eng.* **2015**, *23*, 868–872. [CrossRef]
62. Wang, G.Q.; Xu, O.G.; Xu, Z.C.; Ji, J.B. New HIGEE-Rotating Zigzag Bed and Its Mass Transfer Performance. *Ind. Eng. Chem. Res.* **2008**, *47*, 8840–8846. [CrossRef]
63. Lin, C.C.; Chen, B.C.; Chen, Y.S.; Hsu, S.K. Feasibility of a Cross-Flow Rotating Packed Bed in Removing Carbon Dioxide from Gaseous Streams. *Sep. Purif. Technol.* **2008**, *62*, 507–512. [CrossRef]
64. Kapitza, P.L. Rectification Apparatus. U.S. Patent 2,593,763, 22 April 1952.
65. Visscher, F.; Van Der Schaaf, J.; Nijhuis, T.A.; Schouten, J.C. Rotating Reactors-A Review. *Chem. Eng. Res. Des.* **2013**, *91*, 1923–1940. [CrossRef]
66. Wang, Z.; Yang, T.; Liu, Z.; Wang, S.; Gao, Y.; Wu, M. Mass Transfer in a Rotating Packed Bed: A Critical Review. *Chem. Eng. Process. Process Intensif.* **2019**, *139*, 78–94. [CrossRef]
67. Wang, G.Q.; Zhou, Z.J.; Li, Y.M.; Ji, J.B. Qualitative relationships between structure and performance of rotating zigzag bed in distillation. *Chem. Eng. Process. Process Intensif.* **2019**, *135*, 141–147. [CrossRef]
68. Chu, G.W.; Luo, Y.; Xing, Z.Y.; Sang, L.; Zou, H.K.; Shao, L.; Chen, J.F. Mass-Transfer Studies in a Novel Multiliquid-Inlet Rotating Packed Bed. *Ind. Eng. Chem. Res.* **2014**, *53*, 18580–18584. [CrossRef]
69. Liu, Y.; Zhang, F.; Gu, D.; Qi, G.; Jiao, W.; Chen, X. Gas-Phase Mass Transfer Characteristics in a Counter Airflow Shear Rotating Packed Bed. *Can. J. Chem. Eng.* **2014**, *53*, 18580–18584. [CrossRef]
70. Chamchan, N.; Chang, J.Y.; Hsu, H.C.; Kang, J.L.; Wong, D.S.H.; Jang, S.S.; Shen, J.F. Comparison of Rotating Packed Bed and Packed Bed Absorber in Pilot Plant and Model Simulation for CO_2 Capture. *J. Taiwan Inst. Chem. Eng.* **2017**, *73*, 20–26. [CrossRef]
71. Yu, C.H.; Chen, M.T.; Chen, H.; Tan, C.S. Effects of Process Configurations for Combination of Rotating Packed Bed and Packed Bed on CO_2 Capture. *Appl. Energy* **2016**, *175*, 269–276. [CrossRef]
72. Zhao, B.; Tao, W.; Zhong, M.; Su, Y.; Cui, G. Process, Performance and Modeling of CO_2 Capture by Chemical Absorption Using High Gravity: A Review. *Renew. Sustain. Energy Rev.* **2016**, *65*, 44–56. [CrossRef]
73. Saha, D. Prediction of Mass Transfer Coefficient in Rotating Bed Contactor (Higee) Using Artificial Neural Network. *Heat Mass Transf.* **2009**, *45*, 451–457. [CrossRef]
74. Lashkarbolooki, M.; Vaferi, B.; Mowla, D. Using Artificial Neural Network to Predict the Pressure Drop in a Rotating Packed Bed. *Sep. Sci. Technol.* **2012**, *47*, 2450–2459. [CrossRef]
75. Zhao, B.; Su, Y.; Tao, W. Mass Transfer Performance of CO_2 Capture in Rotating Packed Bed: Dimensionless Modeling and Intelligent Prediction. *Appl. Energy* **2014**, *136*, 132–142. [CrossRef]
76. Li, W.; Wei, S.; Jiao, W.; Qi, G.; Liu, Y. Modelling of Adsorption in Rotating Packed Bed Using Artificial Neural Networks (ANN). *Chem. Eng. Res. Des.* **2016**, *114*, 89–95. [CrossRef]
77. Liu, Z.W.; Liang, F.N.; Liu, Y.Z. Artificial Neural Network Modeling of Biosorption Process Using Agricultural Wastes in a Rotating Packed Bed. *Appl. Therm. Eng.* **2018**, *140*, 95–101. [CrossRef]
78. Liu, T.; Liu, Y.; Wang, D.; Li, Y.; Shao, L. Artificial neural network modeling on the prediction of mass transfer coefficient for ozone absorption in RPB. *Chem. Eng. Res. Des.* **2019**, *152*, 38–47. [CrossRef]
79. Mirzaei, S.; Shamiri, A.; Aroua, M.K. A review of different solvents, mass transfer, and hydrodynamics for postcombustion CO_2 capture. *Rev. Chem. Eng.* **2015**, *31*, 521–561. [CrossRef]
80. Neumann, K.; Hunold, S.; Skiborowski, M.; Górak, A. Dry Pressure Drop in Rotating Packed Beds-Systematic Experimental Studies. *Ind. Eng. Chem. Res.* **2017**, *56*, 12395–12405. [CrossRef]
81. Hendry, J.R.; Lee, J.G.M.; Attidekou, P.S. Pressure Drop and Flooding in Rotating Packed Beds. *Chem. Eng. Process. Process Intensif.* **2020**, *151*, 107908. [CrossRef]
82. Burns, J.R.; Ramshaw, C. Process Intensification: Visual Study of Liquid Maldistribution in Rotating Packed Beds. *Chem. Eng. Sci.* **1996**, *51*, 1347–1352. [CrossRef]
83. Yang, Y.; Xiang, Y.; Chu, G.; Zou, H.; Luo, Y.; Arowo, M.; Chen, J.F. A Noninvasive X-ray Technique for Determination of Liquid Holdup in a Rotating Packed Bed. *Chem. Eng. Sci.* **2015**, *138*, 244–255. [CrossRef]
84. Kelleher, T.; Fair, J.R. Distillation Studies in a High-Gravity Contactor. *Ind. Eng. Chem. Res.* **1996**, *35*, 4646–4655. [CrossRef]
85. Vásquez, P.A.S.; Costa, F.E.; Rela, P.R.; Calvo, W.A.P.; LeRoux, G.A.C.; Hamada, M.M. Gamma Scanning Evaluation for Random Packed Columns. In Proceedings of the IEEE Nuclear Science Symposium Conference Record, Fajardo, PR, USA, 23–29 October 2005. [CrossRef]
86. Aferka, S.; Viva, A.; Brunazzi, E.; Marchot, P.; Crine, M.; Toye, D. Tomographic Measurement of Liquid Hold up and Effective Interfacial Area Distributions in a Column Packed with High Performance Structured Packings. *Chem. Eng. Sci.* **2011**, *66*, 3413–3422. [CrossRef]

87. Gao, X.Y.; Chu, G.W.; Ouyang, Y.; Zou, H.K.; Luo, Y.; Xiang, Y.; Chen, J.F. Gas Flow Characteristics in a Rotating Packed Bed by Particle Image Velocimetry Measurement. *Ind. Eng. Chem. Res.* **2017**, *56*, 14350–14361. [CrossRef]
88. Shoji, E.; Yamagiwa, K.; Kubo, M.; Tsukada, T.; Takami, S.; Sugimoto, K.; Ito, D.; Saito, Y.; Teratani, S. Flow Visualization of Heavy Oil in a Packed Bed Using Real-Time Neutron Radiography. *Chem. Eng. Sci.* **2019**, *196*, 425–432. [CrossRef]
89. Li, H.; Yuan, Z.; Liu, Y.; Liu, H. Characteristics of Liquid Flow in a Countercurrent Rotating Bed. *Chem. Eng. Process. Process Intensif.* **2019**, *136*, 72–81. [CrossRef]
90. Li, X.; Liu, Y. Characteristics of Fin Baffle Packing Used in Rotating Packed Bed. *Chin. J. Chem. Eng.* **2010**, *18*, 55–60. [CrossRef]
91. Sang, L.; Luo, Y.; Chu, G.W.; Zhang, J.P.; Xiang, Y.; Chen, J.F. Liquid Flow Pattern Transition, Droplet Diameter and Size Distribution in the Cavity Zone of a Rotating Packed Bed: A Visual Study. *Chem. Eng. Sci.* **2017**, *158*, 429–438. [CrossRef]
92. Burns, J.R.; Jamil, J.N.; Ramshaw, C. Process Intensification: Operating Characteristics of Rotating Packed Beds-Determination of Liquid Hold-Up for a High-Voidage Structured Packing. *Chem. Eng. Sci.* **2000**, *55*, 2401–2415. [CrossRef]
93. Lin, C.C.; Chen, Y.S.; Liu, H.S. Prediction of Liquid Holdup in Countercurrent-Flow Rotating Packed Bed. *Chem. Eng. Res. Des.* **2000**, *78*, 397–403. [CrossRef]
94. Yi, F.; Zou, H.K.; Chu, G.W.; Shao, L.; Chen, J.F. Modeling and Experimental Studies on Absorption of CO_2 by Benfield Solution in Rotating Packed Bed. *Chem. Eng. J.* **2009**, *145*, 377–384. [CrossRef]
95. Li, W.; Wu, W.; Zou, H.; Chu, G.; Shao, L.; Chen, J. Process Intensification of VOC Removal from High Viscous Media by Rotating Packed Bed. *Chin. J. Chem. Eng.* **2009**, *17*, 389–393. [CrossRef]
96. Xiang, Y.; Wen, L.; Chu, G.; Shao, L.; Xiao, G.; Chen, J. Modeling of the Precipitation Process in a Rotating Packed Bed and Its Experimental Validation. *Chin. J. Chem. Eng.* **2010**, *18*, 249–257. [CrossRef]
97. Sang, L.; Luo, Y.; Chu, G.W.; Sun, B.C.; Zhang, L.L.; Chen, J.F. A Three-Zone Mass Transfer Model for a Rotating Packed Bed. *AIChE J.* **2019**, *65*. [CrossRef]
98. Wang, D.; Liu, T.; Ma, L.; Wang, F.; Shao, L. Modeling and Experimental Studies on Ozone Absorption into Phenolic Solution in a Rotating Packed Bed. *Ind. Eng. Chem. Res.* **2019**, *58*, 7052–7062. [CrossRef]
99. Su, M.J.; Le, Y.; Chu, G.W.; Li, Y.B.; Zhang, L.L.; Luo, Y. Intensification of Droplet Dispersion by Using Multilayer Wire Mesh and Its Application in a Rotating Packed Bed. *Ind. Eng. Chem. Res.* **2020**, *59*, 3584–3592. [CrossRef]
100. Hacking, J.A.; Delsing, N.F.E.J.; de Beer, M.M.; van der Schaaf, J. Improving Liquid Distribution in a Rotating Packed Bed. *Chem. Eng. Process. Process Intensif.* **2020**, *149*, 107861. [CrossRef]
101. Razi, N.; Bolland, O.; Svendsen, H. Review of Design Correlations for CO_2 Absorption into *MEA* Using Structured Packings. *Int. J. Greenh. Gas Control* **2012**, *9*, 193–219. [CrossRef]
102. Suess, P.; Spiegel, L. Hold-up of Mellapak Structured Packings. *Chem. Eng. Process. Process Intensif.* **1992**, *31*, 119–124. [CrossRef]
103. Wolf-Zöllner, V.; Seibert, F.; Lehner, M. Extended Performance Comparison of Different Pressure Drop, Hold-up and Flooding Point Correlations for Packed Columns. *Chem. Eng. Res. Des.* **2019**, *147*, 699–708. [CrossRef]
104. Muzen, A.; Cassanello, M.C. Liquid Holdup in Columns Packed with Structured Packings: Countercurrent vs. Cocurrent Operation. *Che. Eng. Sci.* **2005**, *60*, 6226–6234. [CrossRef]
105. Alix, P.; Raynal, L. Liquid Distribution and Liquid Hold-up in Modern High Capacity Packings. *Chem. Eng. Res. Des.* **2008**, *86*, 585–591. [CrossRef]
106. Lashkarbolooki, M. A General Model for Pressure Drop Prediction across a Rotating Packed Bed. *Sep. Sci. Technol.* **2017**, *52*, 1843–1851. [CrossRef]
107. Bašić, A.; Duduković, M.P. Liquid Holdup in Rotating Packed Beds: Examination of the Film Flow Assumption. *AIChE J.* **1995**, *41*, 301–316. [CrossRef]
108. Piché, S.; Larachi, F.; Grandjean, B.P.A. Improved Liquid Hold-up Correlation for Randomly Packed Towers. *Chem. Eng. Res. Des.* **2001**, *79*, 71–80. [CrossRef]
109. Liu, W.; Chu, G.W.; Luo, Y.; Liu, Y.Z.; Meng, F.Y.; Sun, B.C.; Chen, J.F. Mass Transfer in a Rotating Packed Bed Reactor with a Mesh-Pin Rotor: Modeling and Experimental Studies. *Chem. Eng. J.* **2019**, *369*, 600–610. [CrossRef]
110. Guo, K.; Guo, F.; Feng, Y.; Chen, J.; Zheng, C.; Gardner, N.C. Synchronous Visual and RTD Study on Liquid Flow in Rotating Packed-Bed Contractor. *Chem. Eng. Sci.* **2000**, *55*, 1699–1706. [CrossRef]
111. Xinlin, D.; Xiaoyong, H.; Yigang, D.; Yuanxin, W.; Dinghuo, L. A Model for the Mass Transfer Coefficient in Rotating Packed Bed. *Chem. Eng. Commun.* **2000**, *178*, 249–256. [CrossRef]
112. Rao, D.P.; Bhowal, A.; Goswami, P.S. Process Intensification in Rotating Packed Beds (HIGEE): An Appraisal. *Ind. Eng. Chem. Res.* **2004**, *43*, 1150–1162. [CrossRef]
113. Sivakumar, S.V.; Kaistha, N.; Rao, D.P. Innovations for Process Intensification in the Process Industry. 2004. Available online: https://www.rgipt.ac.in/oldsite/author_doc/S%20-%20122%20.pdf (accessed on 19 February 2021).
114. Neumann, K.; Hunold, S.; Groß, K.; Górak, A. Experimental Investigations on the Upper Operating Limit in Rotating Packed Beds. *Chem. Eng. Process. Process Intensif.* **2017**, *121*, 240–247. [CrossRef]
115. Li, Y.; Lu, Y.; Wang, G.; Nie, Y.; Ying, H.; Ji, J.; Liu, X. Liquid Entrainment and Flooding in a Rotating Zigzag Bed. *Ind. Eng. Chem. Res.* **2015**, *54*, 2554–2563. [CrossRef]
116. Kuźniewska-Lach, I. Estimation of Phase Velocities at Flooding Point in Packed Columns for Any Gas/Liquid System. *Can. J. Chem. Eng.* **1999**, *77*, 439–446. [CrossRef]

117. Stankiewicz, A.; Moulijn, J.A. *Re-Engineering the Chemical Processing Plant*, 1st ed.; CRC Press: Boca Raton, FL, USA, 2003. [CrossRef]
118. Lockett, M.J.; Victor, R.A.; Billingham, J.F. *Structured Packing Flooding: Its Measurement and Prediction, 8th Conference of Distillation and Absorption*; Symposium Series 152; IChemE: London, UK, 2006; pp. 400–408. ISBN 0852955057.
119. Singh, S.P.; Counce, R.M.; Wilson, J.H.; Villiers-Fisher, J.F.; Jennings, H.L.; Lucero, A.J.; Reed, G.D.; Ashworth, R.A.; Elliott, M.G. Removal of Volatile Organic Compounds from Groundwater Using a Rotary Air Stripper. *Ind. Eng. Chem. Res.* **1992**, *31*, 574–580. [CrossRef]
120. Lockett, M.J. Flooding of Rotating Structured Packing and Its Application to Conventional Packed Columns. *Chem. Eng. Res. Des.* **1995**, *73*, 379–384.
121. Rajan, S.; Kumar, M.; Ansari, M.J.; Rao, D.P.; Kaistha, N. Limiting Gas Liquid Flows and Mass Transfer in a Novel Rotating Packed Bed (HiGee). *Ind. Eng. Chem. Res.* **2011**, *50*, 986–997. [CrossRef]
122. Gudena, K.; Rangaiah, G.P.; Lakshminarayanan, S. Optimal Design of a Rotating Packed Bed for VOC Stripping from Contaminated Groundwater. *Ind. Eng. Chem. Res.* **2011**, *51*, 835–847. [CrossRef]
123. Li, S.; Deng, S.; Zhao, L.; Zhao, R.; Lin, M.; Du, Y.; Lian, Y. Mathematical Modeling and Numerical Investigation of Carbon Capture by Adsorption: Literature Review and Case Study. *Appl. Energy* **2018**, *221*, 437–449. [CrossRef]
124. Kumar, M.P.; Rao, D.P. Studies on a High-Gravity Gas-Liquid Contactor. *Ind. Eng. Chem. Res.* **1990**, *29*, 917–920. [CrossRef]
125. Foumeny, E.A.; Kulkarni, A.; Roshani, S.; Vatani, A. Elucidation of Pressure Drop in Packed-Bed Systems. *Appl. Therm. Eng.* **1996**, *16*, 195–202. [CrossRef]
126. Chandra, A.; Goswami, P.S.; Rao, D.P. Characteristics of Flow in a Rotating Packed Bed (HIGEE) with Split Packing. *Ind. Eng. Chem. Res.* **2005**, *44*, 4051–4060. [CrossRef]
127. Sung, W.D.; Chen, Y.S. Characteristics of a Rotating Packed Bed Equipped with Blade Packings and Baffles. *Sep. Purif. Technol.* **2012**, *93*, 52–58. [CrossRef]
128. Wang, G.Q.; Jiao, Y.Q.; Xu, Z.C.; Ji, J.B. Studies on Performance of Crossflow Concentric-Ring Rotating Bed. *Ind. Eng. Chem. Res.* **2009**, *48*, 10643–10649. [CrossRef]
129. Llerena-Chavez, H.; Larachi, F. Analysis of Flow in Rotating Packed Beds via CFD Simulations-Dry Pressure Drop and Gas Flow Maldistribution. *Chem. Eng. Sci.* **2009**, *64*, 2113–2126. [CrossRef]
130. Jiao, W.Z.; Liu, Y.Z.; Qi, G.S. Gas Pressure Drop and Mass Transfer Characteristics in a Cross-Flow Rotating Packed Bed with Porous Plate Packing. *Ind. Eng. Chem. Res.* **2010**, *49*, 3732–3740. [CrossRef]
131. Li, Y.; Ji, J.; Xu, Z.; Wang, G.; Li, X.; Liu, X. Pressure Drop Model on Rotating Zigzag Bed as a New High-Gravity Technology. *Ind. Eng. Chem. Res.* **2013**, *52*, 4638–4649. [CrossRef]
132. Treybal, R.E. *Mass-Transfer Operations*, 3rd ed.; McGraw-Hill Book Company: London, UK, 1980. [CrossRef]
133. Tan, L.S.; Shariff, A.M.; Lau, K.K.; Bustam, M.A. Factors Affecting CO_2 Absorption Efficiency in Packed Column: A Review. *J. Ind. Eng. Chem.* **2012**, *18*, 1874–1883. [CrossRef]
134. Reddy, K.J.; Gupta, A.; Rao, D.P.; Rama, O.P. Process Intensification in a HIGEE with Split Packing. *Ind. Eng. Chem. Res.* **2006**, *45*, 4270–4277. [CrossRef]
135. Tung, H.H.; Mah, R.S.H. Modeling Liquid Mass Transfer in Higee Separation Process. *Chem. Eng. Commun.* **1985**, *39*, 147–153. [CrossRef]
136. Kang, J.L.; Sun, K.; Wong, D.S.H.; Jang, S.S.; Tan, C.S. Modeling Studies on Absorption of CO_2 by Monoethanolamine in Rotating Packed Bed. *Int. J. Greenh. Gas Control* **2014**, *25*, 141–150. [CrossRef]
137. Joel, A.S.; Wang, M.; Ramshaw, C. Modelling and Simulation of Intensified Absorber for Post-Combustion CO_2 Capture Using Different Mass Transfer Correlations. *Appl. Therm. Eng.* **2015**, *74*, 47–53. [CrossRef]
138. Oko, E.; Wang, M.; Ramshaw, C. Study of Mass Transfer Correlations for Intensified Absorbers in Post-Combustion CO_2 Capture Based on Chemical Absorption. *Energy Procedia* **2017**, *114*, 1630–1636. [CrossRef]
139. Sun, B.; Zou, H.; Chu, G.; Shao, L.; Zeng, Z.; Chen, J. Determination of Mass-Transfer Coefficient of CO_2 in NH_3 and CO_2 Absorption by Materials Balance in a Rotating Packed Bed. *Ind. Eng. Chem. Res.* **2012**, *51*, 10949–10954. [CrossRef]
140. Yu, C.H.; Wu, T.W.; Tan, C.S. CO_2 Capture by Piperazine Mixed with Non-Aqueous Solvent Diethylene Glycol in a Rotating Packed Bed. *Int. J. Greenh. Gas Control* **2013**, *19*, 503–509. [CrossRef]
141. Yu, C.H.; Cheng, H.H.; Tan, C.S. CO_2 Capture by Alkanolamine Solutions Containing Diethylenetriamine and Piperazine in a Rotating Packed Bed. *Int. J. Greenh. Gas Control* **2012**, *9*, 136–147. [CrossRef]
142. Chu, G.W.; Fei, J.; Cai, Y.; Liu, Y.Z.; Gao, Y.; Luo, Y.; Chen, J.F. Removal of SO_2 with Sodium Sulfite Solution in a Rotating Packed Bed. *Ind. Eng. Chem. Res.* **2018**, *57*, 2329–2335. [CrossRef]
143. Zhang, L.; Wu, S.; Gao, Y.; Sun, B.; Luo, Y.; Zou, H.; Chu, G.; Chen, J. Absorption of SO_2 with Calcium-Based Solution in a Rotating Packed Bed. *Sep. Purif. Technol.* **2019**, *214*, 148–155. [CrossRef]
144. Zhan, J.; Wang, B.; Zhang, L.; Sun, B.C.; Fu, J.; Chu, G.W.; Zou, H. Simultaneous Absorption of H_2S and CO_2 into the M*DEA* + *PZ* Aqueous Solution in a Rotating Packed Bed. *Ind. Eng. Chem. Res.* **2020**, *59*, 8295–8303. [CrossRef]
145. Chen, Y.S.; Liu, H.S. Absorption of VOCs in a Rotating Packed Bed. *Ind. Eng. Chem. Res.* **2002**, *41*, 1583–1588. [CrossRef]
146. Lin, C.C.; Liu, W.T.; Tan, C.S. Removal of Carbon Dioxide by Absorption in a Rotating Packed Bed. *Ind. Eng. Chem. Res.* **2003**, *42*, 2381–2386. [CrossRef]

147. Chen, Y.S.; Lin, C.C.; Liu, H.S. Mass Transfer in a Rotating Packed Bed with Various Radii of the Bed. *Ind. Eng. Chem. Res.* **2005**, *44*, 7868–7875. [CrossRef]
148. Chen, Y.S.; Lin, F.Y.; Lin, C.C.; Tai, C.Y.D.; Liu, H.S. Packing Characteristics for Mass Transfer in a Rotating Packed Bed. *Ind. Eng. Chem. Res.* **2006**, *45*, 6846–6853. [CrossRef]
149. Chen, Q.Y.; Chu, G.W.; Luo, Y.; Sang, L.; Zhang, L.L.; Zou, H.K.; Chen, J.F. Polytetrafluoroethylene Wire Mesh Packing in a Rotating Packed Bed: Mass-Transfer Studies. *Ind. Eng. Chem. Res.* **2016**, *55*, 11606–11613. [CrossRef]
150. Chen, T.L.; Chen, Y.H.; Chiang, P.C. Enhanced Performance on Simultaneous Removal of NOx-SO_2-CO_2 Using a High-Gravity Rotating Packed Bed and Alkaline Wastes towards Green Process Intensification. *Chem. Eng. J.* **2020**, *393*, 124678. [CrossRef]
151. Luo, Y.; Chu, G.W.; Zou, H.K.; Wang, F.; Xiang, Y.; Shao, L.; Chen, J.F. Mass Transfer Studies in a Rotating Packed Bed with Novel Rotors: Chemisorption of CO_2. *Ind. Eng. Chem. Res.* **2012**, *51*, 9164–9172. [CrossRef]
152. Yang, K.; Chu, G.; Zou, H.; Sun, B.; Shao, L.; Chen, J.F. Determination of the Effective Interfacial Area in Rotating Packed Bed. *Chem. Eng. J.* **2011**, *168*, 1377–1382. [CrossRef]
153. Guo, K.; Zhang, Z.; Luo, H.; Dang, J.; Qian, Z. An Innovative Approach of the Effective Mass Transfer Area in the Rotating Packed Bed. *Ind. Eng. Chem. Res.* **2014**, *53*, 4052–4058. [CrossRef]
154. Luo, Y.; Luo, J.Z.; Chu, G.W.; Zhao, Z.Q.; Arowo, M.; Chen, J.F. Investigation of Effective Interfacial Area in a Rotating Packed Bed with Structured Stainless Steel Wire Mesh Packing. *Chem. Eng. Sci.* **2017**, *170*, 347–354. [CrossRef]
155. Lin, C.C.; Jian, G.S. Characteristics of a Rotating Packed Bed Equipped with Blade Packings. *Sep. Purif. Technol.* **2007**, *54*, 51–60. [CrossRef]
156. Lin, C.C.; Wei, T.Y.; Liu, W.T.; Shen, K.P. Removal of VOCs from Gaseous Streams in a High-Voidage Rotating Packed Bed. *J. Chem. Eng. Japan* **2004**, *37*, 1471–1477. [CrossRef]
157. Chen, Y.S.; Lin, C.C.; Liu, H.S. Mass Transfer in a Rotating Packed Bed with Viscous Newtonian and Non-Newtonian Fluids. *Ind. Eng. Chem. Res.* **2005**, *44*, 1043–1051. [CrossRef]
158. Chen, Y.S. Correlations of Mass Transfer Coefficients in a Rotating Packed Bed. *Ind. Eng. Chem. Res.* **2011**, *50*, 1778–1785. [CrossRef]
159. Bai, S.; Chu, G.-W.; Li, S.-C.; Zou, H.-K.; Xiang, Y.; Luo, Y.; Chen, J.-F. SO_2 Removal in a Pilot Scale Rotating Packed Bed. *Environ. Eng. Sci.* **2015**, *32*, 806–815. [CrossRef]
160. Mei-ying, D.; Gui-sheng, Q.; You-zhi, L.; Qiang, G.; Song Bin, W.T. Experimental Study on Influential Factors of Mass Transfer in a Cross-Flow Rotating Packed Bed. *Chin. J. Process Eng.* **2015**, *15*, 929–934. [CrossRef]
161. Cao, S.; Liu, P.; Zhang, L.; Sun, B.; Zou, H.; Chu, G.; Luo, Y.; Chen, J. Mass Transfer Study of Dehydration by Triethylene Glycol in Rotating Packed Bed for Natural Gas Processing. *Ind. Eng. Chem. Res.* **2018**. [CrossRef]
162. Su, M.J.; Luo, Y.; Chu, G.W.; Liu, W.; Zheng, X.H.; Chen, J.F. Gas-Side Mass Transfer in a Rotating Packed Bed with Structured Nickel Foam Packing. *Ind. Eng. Chem. Res.* **2018**, *57*, 5394–5400. [CrossRef]
163. Li, W.; Liu, H.; Li, S.; Li, W.; Chen, Y.; Gao, J.; Cao, Y. Removal of Hydrophobic Volatile Organic Compounds with Sodium Hypochlorite and Surfactant in a Co-Current Rotating Packed Bed. *J. Environ. Sci.* **2018**, *64*, 190–196. [CrossRef]
164. Kolev, N. *Packed Bed Columns: For Absorption, Desorption, Rectification and Direct Heat Transfer*; Elsevier Science: Amsterdam, The Netherlands, 2006. [CrossRef]
165. Wagner, I.; Stichlmair, J.; Fair, J.R. Mass Transfer in Beds of Modern, High-Efficiency Random Packings. *Ind. Eng. Chem. Res.* **1997**, *36*, 227–237. [CrossRef]
166. Liu, T.; Wang, D.; Wang, W.; Liang, Q.; Shao, L. Study on the Efficient Production of Ozone Water by a Rotating Packed Bed. *Ind. Eng. Chem. Res.* **2019**, *58*, 7227–7232. [CrossRef]
167. Luo, Y.; Chu, G.W.; Zou, H.K.; Zhao, Z.Q.; Dudukovic, M.P.; Chen, J.F. Gas-Liquid Effective Interfacial Area in a Rotating Packed Bed. *Ind. Eng. Chem. Res.* **2012**, *51*, 16320–16325. [CrossRef]
168. Onda, K.; Takeuchi, H.; Okumoto, Y. Mass Transfer Coefficients between Gas and Liquid Phases in Packed Columns. *J. Chem. Eng. Jpn.* **1968**, *1*, 56–62. [CrossRef]
169. Puranik, S.S.; Vogelpohl, A. Effective Interfacial Area in Irrigated Packed Columns. *Chem. Eng. Sci.* **1974**, *29*, 501–507. [CrossRef]
170. Xie, P.; Lu, X.; Ding, H.; Yang, X.; Ingham, D.; Ma, L.; Pourkashanian, M. A Mesoscale 3D CFD Analysis of the Liquid Flow in a Rotating Packed Bed. *Chem. Eng. Sci.* **2019**, *199*, 528–545. [CrossRef]
171. Lu, Y.-Z.; Liu, W.; Xu, Y.-C.; Luo, Y.; Chu, G.-W.; Chen, J.-F. Initial Liquid Dispersion and Mass Transfer Performance in a Rotating Packed Bed. *Chem. Eng. Process. Process Intensif.* **2019**, *140*, 136–141. [CrossRef]
172. Sheng, M.; Sun, B.; Zhang, F.; Chu, G.; Zhang, L.; Liu, C.; Chen, J.-F.; Zou, H. Mass-Transfer Characteristics of the CO_2 Absorption Process in a Rotating Packed Bed. *Energy Fuels* **2015**, *30*, 4215–4220. [CrossRef]
173. Yang, Y.C.; Ouyang, Y.; Zhang, N.; Yu, Q.J.; Arowo, M. A Review on Computational Fluid Dynamic Simulation for Rotating Packed Beds. *J. Chem. Technol. Biotechnol.* **2019**, *94*, 1017–1031. [CrossRef]
174. Lu, X.; Xie, P.; Ingham, D.B.; Ma, L.; Pourkashanian, M. A Porous Media Model for CFD Simulations of Gas-Liquid Two-Phase Flow in Rotating Packed Beds. *Chem. Eng. Sci.* **2018**, *189*, 123–134. [CrossRef]
175. Liu, Y.; Wu, W.; Luo, Y.; Chu, G.W.; Liu, W.; Sun, B.C.; Chen, J.F. CFD Simulation and High-Speed Photography of Liquid Flow in the Outer Cavity Zone of a Rotating Packed Bed Reactor. *Ind. Eng. Chem. Res.* **2019**, *58*, 5280–5290. [CrossRef]
176. Yang, W.; Wang, Y.; Chen, J.; Fei, W. Computational Fluid Dynamic Simulation of Fluid Flow in a Rotating Packed Bed. *Chem. Eng. J.* **2010**, *156*, 582–587. [CrossRef]

177. Martínez, E.L.; Jaimes, R.; Gomez, J.L.; Filho, R.M. CFD Simulation of Three-Dimensional Multiphase Flow in a Rotating Packed Bed. In *Computer Aided Chemical Engineering*; Elsevier BV: Amsterdam, The Netherlands, 2012. [CrossRef]
178. Shi, X.; Xiang, Y.; Wen, L.X.; Chen, J.F. CFD Analysis of Liquid Phase Flow in a Rotating Packed Bed Reactor. *Chem. Eng. J.* **2013**, *228*, 1040–1049. [CrossRef]
179. Chengcheng, X.; Weizhou, J.; Youzhi, L.; Liang, G.; Zhiguo, Y.; Qiaoling, Z. Effects of Airflow Field on Droplets Diameter inside the Corrugated Packing of a Rotating Packed Bed. *China Pet. Process. Petrochem. Technol.* **2014**, *16*, 38–46.
180. Sun, Y.; Zhang, Y.; Zhang, L.; Jiang, B.; Zhao, Z. Structure Optimization of a Rotating Zigzag Bed via Computational Fluid Dynamics Simulation. *Ind. Eng. Chem. Res.* **2014**, *53*, 13764–13772. [CrossRef]
181. Yang, Y.; Xiang, Y.; Chu, G.; Zou, H.; Sun, B.; Arowo, M.; Chen, J.F. CFD Modeling of Gas-Liquid Mass Transfer Process in a Rotating Packed Bed. *Chem. Eng. J.* **2016**, *294*, 111–121. [CrossRef]
182. Gao, X.Y.; Liu, L.; Hu, M.L.; Xiang, Y.; Chu, G.W.; Zou, H.K.; Sun, B.C.; Chen, J.F. Numerical Simulation for Mass Transfer Characteristics of CO_2 Capture in a Rotating Packed Bed. *Chem. Eng. Process. Process Intensif.* **2016**, *109*, 68–79. [CrossRef]
183. Liu, Y.; Luo, Y.; Chu, G.W.; Luo, J.Z.; Arowo, M.; Chen, J.F. 3D Numerical Simulation of a Rotating Packed Bed with Structured Stainless Steel Wire Mesh Packing. *Chem. Eng. Sci.* **2017**, *170*, 365–377. [CrossRef]
184. Hu, D.D.; Shan, W.Y.; Zhu, G.W. Numerical Simulation of Counter-Current Flow Field in Double Packing Rotating Packed Bed. *Key Eng. Mater.* **2013**, *561*, 672–676. [CrossRef]
185. Zhang, X.; Cheng, Y.; Nie, S.; Ji, H.; Liu, L. Simulation of Multiphase Flow of the Oil-Water Separation in a Rotating Packed Bed for Oil Purification. *Math. Probl. Eng.* **2013**, *2013*, 1–9. [CrossRef]
186. Guo, T.Y.; Shi, X.; Chu, G.W.; Xiang, Y.; Wen, L.X.; Chen, J.F. Computational Fluid Dynamics Analysis of the Micromixing Efficiency in a Rotating-Packed-Bed Reactor. *Ind. Eng. Chem. Res.* **2016**, *55*, 4856–4866. [CrossRef]
187. Xie, P.; Lu, X.; Ingham, D.; Ma, L.; Pourkashanian, M. Mass Transfer Characteristics of the Liquid Film Flow in a Rotating Packed Bed for CO_2 Capture: A Micro-Scale CFD Analysis. *Energy Procedia* **2017**, *142*, 3407–3414. [CrossRef]
188. Xie, P.; Lu, X.; Yang, X.; Ingham, D.; Ma, L.; Pourkashanian, M. Characteristics of Liquid Flow in a Rotating Packed Bed for CO_2 Capture: A CFD Analysis. *Chem. Eng. Sci.* **2017**, *172*, 216–229. [CrossRef]
189. Guo, T.-Y.; Cheng, K.-P.; Wen, L.-X.; Andersson, R.; Chen, J.-F. Three-Dimensional Simulation on Liquid Flow in a Rotating Packed Bed Reactor. *Ind. Eng. Chem. Res.* **2017**, *56*, 8169–8179. [CrossRef]
190. Ouyang, Y.; Xiang, Y.; Gao, X.Y.; Li, W.L.; Zou, H.K.; Chu, G.W.; Chen, J.F. Micromixing Efficiency in a Rotating Packed Bed with Non-Newtonian Fluid. *Chem. Eng. J.* **2018**, *354*, 162–171. [CrossRef]
191. Wu, W.; Luo, Y.; Chu, G.W.; Liu, Y.; Zou, H.K.; Chen, J.F. Gas Flow in a Multiliquid-Inlet Rotating Packed Bed: Three-Dimensional Numerical Simulation and Internal Optimization. *Ind. Eng. Chem. Res.* **2018**, *57*, 2031–2040. [CrossRef]
192. Ouyang, Y.; Wang, S.; Xiang, Y.; Zhao, Z.; Wang, J.; Shao, L. CFD Analyses of Liquid Flow Characteristics in a Rotor-Stator Reactor. *Chem. Eng. Res. Des.* **2018**, *134*, 186–197. [CrossRef]
193. Wang, Z.; Wu, X.; Yang, T.; Wang, S.; Liu, Z.; Dan, X. Droplet Characteristics of Rotating Packed Bed in H2S Absorption: A Computational Fluid Dynamics Analysis. *Processes* **2019**, *7*, 724. [CrossRef]
194. Wu, W.; Luo, Y.; Chu, G.W.; Su, M.J.; Cai, Y.; Zou, H.K.; Chen, J.F. Liquid Flow Behavior in a Multiliquid-Inlet Rotating Packed Bed Reactor with Three-Dimensional Printed Packing. *Chem. Eng. J.* **2020**, *386*, 121537. [CrossRef]
195. Ouyang, Y.; Xiang, Y.; Gao, X.-Y.; Zou, H.-K.; Chu, G.-W.; Agarwal, R.K.; Chen, J.-F. Micromixing Efficiency Optimization of the Premixer of a Rotating Packed Bed by CFD. *Chem. Eng. Process.Process Intensif.* **2019**, *142*, 107543. [CrossRef]
196. Liu, Y.; Luo, Y.; Chu, G.W.; Larachi, F.; Zou, H.K.; Chen, J.F. Liquid Microflow inside the Packing of a Rotating Packed Bed Reactor: Computational, Observational and Experimental Studies. *Chem. Eng. J.* **2020**, *386*, 121134. [CrossRef]
197. Xu, Y.C.; Li, Y.B.; Liu, Y.Z.; Luo, Y.; Chu, G.W.; Zhang, L.L.; Chen, J.F. Liquid Jet Impaction on the Single-Layer Stainless Steel Wire Mesh in a Rotating Packed Bed Reactor. *AIChE J.* **2019**, *65*. [CrossRef]
198. Wang, J.Q.; Ouyang, Y.; Li, W.L.; Esmaeili, A.; Xiang, Y.; Chen, J.F. CFD Analysis of Gas Flow Characteristics in a Rotating Packed Bed with Randomly Arranged Spherical Packing. *Chem. Eng. J.* **2020**, *385*, 123812. [CrossRef]
199. Harmsen, G.J. Reactive Distillation: The Front-Runner of Industrial Process Intensification. A Full Review of Commercial Applications, Research, Scale-up, Design and Operation. *Chem. Eng. Process. Process Intensif.* **2007**, *46*, 774–780. [CrossRef]
200. Khang, S.J.; Levenspiel, O. New Scale-up and Design Method for Stirrer Agitated Batch Mixing Vessels. *Chem. Eng. Sci.* **1976**, *31*, 569–577. [CrossRef]
201. Kapic, A.; Heindel, T.J. Correlating Gas-Liquid Mass Transfer in a Stirred-Tank Reactor. *Chem. Eng. Res. Des.* **2006**, *84*, 239–245. [CrossRef]
202. Gui, H.; Li, X. Removing Ammonia from Skim by Air Stripping with Rotating Packed Bed. *Chin. J. Chem. Eng.* **2019**, *27*, 528–533. [CrossRef]
203. Vivian, J.E.; Brian, P.L.T.; Krukonis, V.J. The Influence of Gravitational Force on Gas Absorption in a Packed Column. *AIChE J.* **1965**, *11*, 1088–1091. [CrossRef]
204. Chakravarti, S.A.; Shenoy, U.V. Dimensional Analysis of Heat and Mass Transfer Correlations Using Micro-and Macro Scales. *Chem. Eng. Commun.* **1993**, *124*, 29–37. [CrossRef]
205. Shivhare, M.K.; Rao, D.P.; Kaistha, N. Mass Transfer Studies on Split-Packing and Single-Block Packing Rotating Packed Beds. *Chem. Eng. Process. Process Intensif.* **2013**, *71*, 115–124. [CrossRef]
206. Keyvani, M.; Gardner, N.C. Operating Characteristics of Rotating Beds. *Chem. Eng. Prog.* **1989**, *85*, 48–52.

207. Agarwal, L.; Pavani, V.; Rao, D.P.; Kaistha, N. Process Intensification in HiGee Absorption and Distillation: Design Procedure and Applications. *Ind. Eng. Chem. Res.* **2010**, *49*, 10046–10058. [CrossRef]
208. Jiang, X.; Liu, Y.; Gu, M. Absorption of Sulphur Dioxide with Sodium Citrate Buffer Solution in a Rotating Packed Bed. *Chinese J. Chem. Eng.* **2011**, *19*, 687–692. [CrossRef]
209. Lee, J.; Kolawole, T.; Attidekou, P. Carbon Capture from a Simulated Flue Gas Using a Rotating Packed Bed Adsorber and Mono Ethanol Amine (*MEA*). *Energy Procedia* **2017**, *114*, 1834–1840. [CrossRef]